arXiv:2505.00347v1 [cs.LG] 1 May 2025

Pushing the Limits of Low-Bit Optimizers: A Focus on EMA Dynamics

Cong Xu [1] **Wenbin Liang** [1 2] **Mo Yu** [3] **Anan Liu** [4] **Ke-Yue Zhang** [2] **Lizhuang Ma** [1] **Jianyong Wang** [5]
Jun Wang [1] **Wei Zhang** [1 6]

https://github.com/MTandHJ/SOLO

Abstract

The explosion in model sizes leads to continued growth in prohibitive training/fine-tuning costs, particularly for stateful optimizers which maintain auxiliary information of even 2x the model size to achieve optimal convergence. We therefore present in this work a novel type of optimizer that carries with extremely lightweight state overloads, achieved through ultra-low-precision quantization. While previous efforts have achieved certain success with 8-bit or 4-bit quantization, our approach enables optimizers to operate at precision as low as 3 bits, or even 2 bits per state element. This is accomplished by identifying and addressing two critical challenges: the signal swamping problem in unsigned quantization that results in unchanged state dynamics, and the rapidly increased gradient variance in signed quantization that leads to incorrect descent directions. The theoretical analysis suggests a tailored logarithmic quantization for the former and a precision-specific momentum value for the latter. Consequently, the proposed SOLO achieves substantial memory savings (approximately 45 GB when training a 7B model) with minimal accuracy loss. We hope that SOLO can contribute to overcoming the bottleneck in computational resources, thereby promoting greater accessibility in fundamental research.

1. Introduction

The rapid scaling of model sizes has begun to strain the ongoing advancement of AI across various domains (*e.g.*, Computer Vision (Dosovitskiy et al., 2020; Liu et al., 2023), Natural Language Processing (Radford, 2018; GenAI, 2023), and Recommender Systems (Zhai et al., 2024; Zhang et al., 2024a)). Fundamental AI research is, regrettably, becoming a luxury beyond the reach of most researchers and teams. Recall that modern optimizers typically consume substantial memory to maintain auxiliary information aimed at optimizing and accelerating convergence. For instance, the commonly adopted Adam(W) optimizer (Kingma & Ba, 2015; Loshchilov & Hutter, 2017) necessitates a buffer of 2x model size to track 1st moment (for approximating the signed 'global' descent directions) and 2nd moment (for approximating the unsigned the adaptive learning rates). As illustrated in Figure 1, these maintained states account for nearly half of the total memory usage in a standard mixed-precision training (Micikevicius et al., 2018).

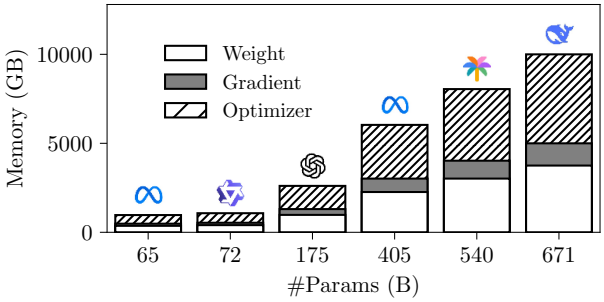

Figure 1. Memory costs of various LLMs, from left to right including Touvron et al. (2023); Yang et al. (2024); Radford (2018); GenAI (2023); Anil et al. (2023); Liu et al. (2024b). The costs are estimated based on a standard mixed-precision training: 1) 16-bit model weights along with a 32-bit copy; 2) 16-bit gradients; 3) 32-bit optimizer states. Other activations and temporary buffers are excluded for simplicity.

Once the optimizer is slimmed down, the saved memory can be reallocated to accommodate a larger model or increased batch size. There are some straightforward *hardware-level* methods to accomplish this, such as GPU sharding (Rajbhandari et al., 2020) and CPU offloading (Ren et al., 2021); however, these solutions are known to struggle with excessive communication overloads (Wang et al., 2023), and are not easy to use in practice. Low-bit optimizers (Dettmers, 2015), which maintain states at low precision, stand out due

[1]East China Normal University [2]Tencent Youtu Lab [3]WeChat AI, Tencent [4]Machine Learning Platform Department, Tencent TEG [5]Tsinghua University [6]Shanghai Innovation Institute. Correspondence to: Cong Xu <congxueric@gmail.com>, Jun Wang <wongjun@gmail.com>, Wei Zhang <zhangwei.thu.2011@gmail.com>.

to their orthogonality to the *model architecture*, *task*, *hardware*, and the aforementioned *distributed algorithms*. For example, about $1/8$ of the memory overhead is enough for an optimizer if the states are maintained in 4-bit instead of the original 32-bit format. Previous efforts have achieved certain success in 8- or 4-bit quantization (Dettmers et al., 2022; Li et al., 2023a), but they just apply regular quantization tricks to minimize the quantization error, overlooking the peculiarities of the optimizer state update. As a result, the existing 4-bit optimizers have a non-negligible performance degradation, not to mention 3-bit or 2-bit precision.

Recall that the Exponential Moving Average (EMA) mechanism with a momentum $\beta \in [0, 1)$ is widely employed in modern optimizers to update state x upon received signal z:

$$x_{t+1} \leftarrow \beta \cdot x_t + (1 - \beta) \cdot z_{t+1}.$$

We demonstrate that some overlooked problems exist when unsigned or signed quantization is directly applied to EMA state updates on the fly:

- Unsigned EMA update is susceptible to a signal *swamping* problem (Higham, 1993; Wang et al., 2018b); that is, the state might keep unchanged regardless of the gap between the newly received signal and the current state value. This problem becomes particularly severe when employing a large momentum ($\beta \to 1$), where the added value of $(1-\beta)z_{t+1}$ becomes very small and is thus easily swamped, even when the incoming signal z_{t+1} is actually large. Since the unsigned EMA update is typically used to estimate adaptive learning rates, the useful adaptivity can no longer kick in once the swamping problem occurs.
- Signed EMA update is highly susceptible to quantization errors due to the additional burden of sign representation and its direct impact on the update direction. Moreover, these quantization errors inherently increase the gradient noise variance, leading to inevitable slowdowns in convergence and even training collapses.

Thanks to these deeper understandings, we are to develop **S**tateful **O**ptimizers in ultra-**LO**w bits (SOLO). To the best of our knowledge, we are the first to point out the feasibility of reducing optimizer precision to as low as 3 or even 2 bits.

- While standard stochastic rounding (Xia et al., 2020) is the straightforward way to escape from strict signal swamping, it is unfortunately accompanied by high variance when quantifying state values close to zero. In order to achieve robust unsigned state quantization, more quantization levels should be allocated near the zero point rather than evenly distributed levels. Hence, the logarithmic quantization (Oh et al., 2021) with a specific base is adopted. It allows for an exact exponential decay with an easy-to-implement stochastic rounding mechanism.
- We derive an upper bound for the gradient noise variance when performing low-bit quantization in signed EMA updates. Since too high a gradient variance impairs training (Li et al., 2023b; Wang et al., 2024), we hypothesize that an acceptable convergence rate can be achieved if the upper bound can be somewhat controlled. It suggests an adjustment of the momentum value β; for instance, if $\beta = 0.9$ performs effectively in 5-bit signed EMA updates already, a reduced value of $\beta \leq 0.820$ is recommended in the 4-bit scenario for an acceptable gradient noise variance. In practical applications, we offer a table as an empirical reference (see Figure 4).

We apply SOLO to the widely used Adam(W) optimizer, giving two variants operating at ultra-low precision. First, we propose the 4/2-bit Adam(W), which performs 4-bit signed and 2-bit unsigned quantization, respectively. This version is equivalent to a 3-bit Adam(W) optimizer in memory savings but allows more stable performance due to a more balanced bit allocation. Second, we develop a 2-bit Adam(W) optimizer to explore the limits of ultra-low-bit optimizers.

The superiority of SOLO has been demonstrated across various domains: (**CV**) Swin-T for image classification; (**NLP**) Transformer-Base for neural machine translation and RoBERTa-Large for natural language understanding; (**RS**) DCN for click-through rate prediction and HSTU-Large for sequential recommendation. Finally, we validate the effectiveness in giant model training, including (**LLM**) LLaMA-7B fine-tuning on Alpaca and (**LVM**) LLaVA-1.5 visual instruction tuning based on CLIP and Vicuna-7B-1.5.

This paper is organized as follows. We begin by reviewing related work, with a focus on efforts to alleviate the 'hardware bottleneck'. Subsequently, we delve into the details of low-bit optimizers and systematically analyze the challenges involved, followed by discussions on feasible solutions. In Section 4, we present a comprehensive comparison between SOLO and other low-precision counterparts, supported by extensive empirical analysis. For clarity, preliminaries on quantization methods and detailed theoretical proofs are provided in Appendix.

2. Related Work

2.1. Efficient Architecture and Parallelism

One of the most straightforward approaches is to redesign the base model (Waswani et al., 2017; Radford, 2018; Gu & Dao, 2023), such as replacing the computationally intensive attention mechanism with alternatives like multi-head latent attention (Liu et al., 2024a) or linear attention (Katharopoulos et al., 2020), or employing Mixture-of-Experts (MoE) architectures (Shazeer et al., 2017). This usually improves

both training and inference efficiency but requires extensive engineering validation. There are some more parameter-efficient fine-tuning techniques (Han et al., 2024), such as soft-prompt on tuning the input (Li & Liang, 2021) and LoRA on low-rank adaptation (Hu et al., 2021). Since only a limited number of parameters are involved in training, the required optimizer states can be significantly reduced.

Data and model parallelism have been widely employed for large-scale model training across multi-GPU clusters. Recent studies have identified their limitations in memory reduction, prompting the development of specialized optimization techniques (Seide et al., 2014). For instance, ZeRO (Rajbhandari et al., 2020) enables efficient partitioning of optimizer states, gradients, and model parameters. Furthermore, ZeRO-Offload (Ren et al., 2021) and ZeRO-Infinity (Rajbhandari et al., 2021) extend this framework by leveraging CPU and NVMe resources, respectively, for enhanced memory utilization. However, these strategies are associated with a non-negligible communication overhead, despite the presence of certain modifications (Wang et al., 2023).

In summary, the aforementioned training strategies are often dependent on specific models or hardware, necessitating additional code refactoring. The low-bit optimizers explored in this study are orthogonal to these approaches and exhibit a broader range of applicability.

2.2. Network Quantization

While model training and inference are typically conducted at full precision (*i.e.*, 32 bits) by default, significant memory savings can be achieved through the application of low-precision quantization (Ashkboos et al., 2024; Zhao et al., 2024b; Frantar et al., 2022). This approach has achieved remarkable success in the inference phase, where the quantization precision can be reduced to as low as 4 (Lin et al., 2024; 2025) with minimal performance degradation by 'smoothing' the activation outliers. As a result, deploying LLMs on personal computers becomes feasible.

However, this is still difficult to apply to Fully Quantized Training (FQT) in a model-independent manner (Zhou et al., 2017; Tang et al., 2022; Xi et al., 2024; 2023). While FP16/BF16 mixed-precision training (Micikevicius et al., 2018) has been extensively validated, the appropriate approach for lower-precision quantization has yet to be thoroughly established. Indeed, the FP8 mixed-precision training has only recently been realized in giant model training (Liu et al., 2024b). Current 4-bit (Sun et al., 2020) and even 1-bit (Gao et al., 2024) FQT methods remain far from practical due to the significant and unacceptable loss in accuracy.

2.3. Lightweight Optimizers

Lightweight optimizers have garnered increasing attention (Shazeer & Stern, 2018; Dettmers et al., 2022; Luo et al., 2024) as traditional stateful optimizers are memory-intensive. Most alternatives aim to simplify the Adam optimizer (Kingma & Ba, 2015) by condensing the 2nd state (Anil et al., 2019), namely the adaptive learning rates on the fly. For instance, Adafactor (Shazeer & Stern, 2018) introduces factored 2nd state estimation, while the recently Adam-mini (Zhang et al., 2024b) observes most entries within a block could share a common 2nd state. In addition, GaLore (Zhao et al., 2024a) attains memory-efficient optimization by conducting state updates in a low-dimensional space. Lion (Chen et al., 2024) relies solely on 1st sign momentum to achieve comparable performance across most tasks.

Although these optimizers are lightweight by design, their generalizability has not been thoroughly validated compared to the widely adopted Adam(W) optimizer. We therefore focus on low-bit optimizers due to their model-, task-, and hardware-agnostic characteristics. They enable seamless deployment following the same procedures as their high-precision counterparts, while substantially reducing the effort required for hyperparameter tuning compared to the aforementioned lightweight optimizers. Moreover, some lightweight optimizers like Adafactor can also benefit from low-bit quantization, further reducing memory consumption. Currently, 8-bit (Dettmers et al., 2022) and 4-bit (Li et al., 2023a) optimizers have been developed, primarily relying on regular quantization tricks such as linear or dynamic exponent mappings. In the following, we analyze how the overlook of the EMA update mechanism hinders the development of ultra-low-bit optimizers.

3. Ultra-Low-Bit Optimizers

It is well known that the auxiliary information maintained by an optimizer contribute substantially to the overall memory cost. For instance, the commonly adopted Adam(W) optimizer (Kingma & Ba, 2015; Loshchilov & Hutter, 2017) necessitates a buffer of 2x model size to track 1st moment (for approximating the signed 'global' descent directions) and 2nd moment (for estimating the unsigned adaptive learning rates), about 520 GB memory usage for a 65B model. In the following, we first elucidate the effectiveness of the low-bit optimizer for addressing this problem, and then systematically analyze the challenges and corresponding solutions when extending to ultra-low-precision scenarios.

3.1. Quantization and Dequantization in EMA Update

The b-bit quantization for a high-precision tensor X aims to map each element $x \in X$ to an integer $q \in \{0, 1, \ldots, 2^b -$

1}. Given the scale factor $\Delta := \max_{x \in X} |x|$, a majority of quantizers can be unified as a *nearest rounding* process:

$$q = Q(x) := \underset{k=0}{\overset{2^b-1}{\operatorname{argmin}}} \left| \frac{x}{\Delta} - y_k \right|. \tag{1}$$

where $y_k,\ k = 0, 1, \ldots, 2^b - 1$ are *monotonic* quantization levels distributed across the interval [0, 1] ([-1, 1]) for unsigned (signed) quantization. For instance, linear quantization is a simple yet effective method, utilizing evenly distributed levels. Intuitively, the resulting quantized value q implies the normalized value x/Δ is closest to the q-th (indexed from 0) level y_q. These low-precision integers, along with a full-precision scale factor, can be stored and subsequently utilized to 'recover' the high-precision tensor:

$$\tilde{x} = Q^{\dagger}(q) := y_q \cdot \Delta.$$

Compared to the original high-precision tensor, the storage of quantized values benefits from reduced memory requirements, albeit at the expense of introducing some quantization (rounding) errors.

Recall that most recent (Adam-style) optimizers rely on the Exponential Moving Average (EMA) for state updates. In the context of low-precision quantization, this process can be divided into three steps:

$$\text{Dequantization: } \tilde{x}_t = Q^{\dagger}(q_t) = y_{q_t} \cdot \Delta_t, \tag{2}$$

$$\text{EMA update: } \hat{x}_{t+1} \leftarrow \beta \cdot \tilde{x}_t + (1-\beta) \cdot z_{t+1}, \tag{3}$$

$$\text{Quantization: } q_{t+1} = Q(\hat{x}_{t+1}), \tag{4}$$

where z_{t+1} is the received signal at $t+1$ update. Taking the Adam optimizer as an example, z_{t+1} corresponds to the gradient g_{t+1} in the *signed* state update and the sqaured gradient g_{t+1}^2 in the *unsigned* state update. We emphasize that the signed and unsigned EMA updates typically serve distinct roles in optimizers. Subsequently, we analyze the respective challenges and propose feasible solutions, beginning with unsigned updates to signed updates.

3.2. Quantization for Unsigned EMA Update

3.2.1. Signal Swamping Problem

Recall that the unsigned EMA update is commonly applied in the denominator to estimate adaptive learning rates. Therefore, the primary goal is to ensure that the $\hat{x}_t$ closely follow the trend of the ground-truth state x_t. Unfortunately, for certain quantization levels y_i with a large radius, the *swamping* problem (Higham, 1993; Wang et al., 2018b), frequently observed in large-to-small number addition, may arise severely. In this case, the received signal is 'swamped' by the current state value, potentially resulting in a constant state, which fundamentally undermines the intended purpose of applying EMA.

Theorem 3.1 (Signal Swamping)**.** *Let y_{q_t} be the closest level to q_t, and its radius be defined by*

$$r = \frac{1}{2} \min \Big\{ |y_{q_t} - y_{q_t - 1}|, |y_{q_t+1} - y_{q_t}| \Big\}.$$

The quantized state q_t remains unchanged if

$$r \geq (1-\beta) \cdot \left| \frac{z_{t+1}}{\Delta_{t+1}} - y_{q_t} \right| + \left| \frac{\Delta_t}{\Delta_{t+1}} - 1 \right|. \tag{5}$$

In other words, if the radius around y_{q_t} is large enough, the state will keep constant even receiving a quite different signal. Four key factors significantly increase the likelihood of the signal swamping problem:

- **Low precision**. A lower precision generally results in a larger radius r since the entire interval must be covered with fewer quantization levels.
- **Large tensor size**. For a larger-size tensor X quantized as a whole, the scale factor $\Delta = \max_{x \in X} |x|$ becomes larger, potentially leading to a smaller value of $|z_{t+1}/\Delta_{t+1} - y_{q_t}|$. Moreover, changes from Δ_t to Δ_{t+1} tend to be negligible, further exacerbating this issue.
- **Unsigned EMA update**. Note that for the signed state update, the accumulation process incorporates both positive and negative values. This results in a mixed state with a much smaller magnitude compared to the signal itself. In this case, the swamping problem is less severe due to a large $|z_{t+1}/\Delta_{t+1}|$ allowed. Conversely, the unsigned EMA update is more prone to signal swamping.
- **Momentum** $\beta \to 1$. A large momentum β has a direct impact on the swamping problem. Notably, the unsigned EMA state update typically employs a larger momentum (*e.g.*, $\beta = 0.999$) compared to the signed EMA update (*e.g.*, $\beta = 0.9$), which further exacerbates the issue in the unsigned EMA update.

To summarize,

> The unsigned EMA update, particularly when employing a large momentum ($\beta \to 1$), is highly susceptible to signal swamping, especially in scenarios involving low precision and large-size tensors.

The impact of signal swamping. The EMA update serves as a dynamic estimation of the expectation $\mathbb{E}[z_t]$ when z_t follows a stationary distribution. Clearly a state undergoing signal swamping cannot be expected to converge to the true expectation value, not to mention the complex state dynamics in practice. In other words, once the swamping problem arises, the cumulative approximation error will inevitably

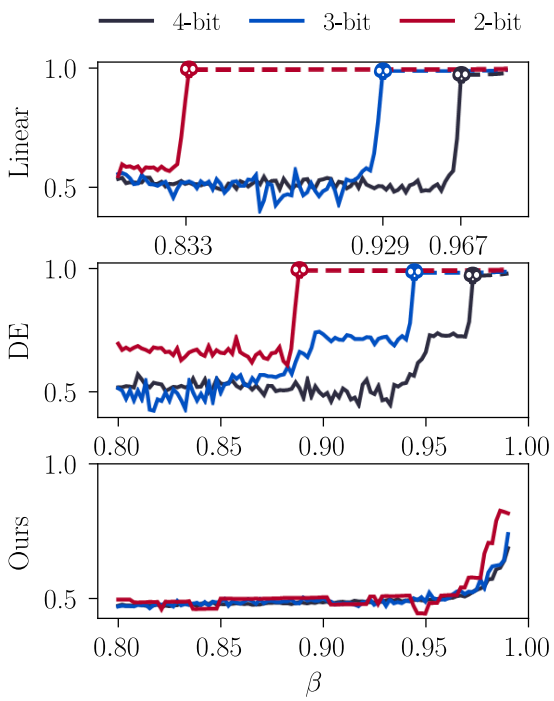

Figure 2. Synthetic uniform signals. $\mathbb{E}[z] = 0.5$ represents the expected value to which the quantized value shall converge.

grow to an unacceptable level. To provide a clearer understanding of this impact, we demonstrate several surprising cases associated with two widely adopted quantization methods. As the unsigned EMA state update is most affected, we present the analysis on *unsigned* quantization and leave a generalized version in Appendix B.

Corollary 3.2. *If $\Delta_{t+1} = \Delta_t$ and $r_t \geq 2(1-\beta)$, the unsigned quantized state q_t remains unchanged for any $z_{t+1} \leq \Delta_t$. To be specific,*

- *For linear quantization, the received signals are swamped by states corresponding to any level when*

$$\beta \gtrapprox \underbrace{0.999}_{\text{8-bit}}, \underbrace{0.967}_{\text{4-bit}}, \underbrace{0.929}_{\text{3-bit}}, \underbrace{0.833}_{\text{2-bit}}. \tag{6}$$

- *For dynamic exponent quantization, the received signals are swamped by states corresponding to half of the levels when*

$$\beta \gtrapprox \underbrace{0.998}_{\text{8-bit}}, \underbrace{0.966}_{\text{4-bit}}, \underbrace{0.933}_{\text{3-bit}}, \underbrace{0.837}_{\text{2-bit}}. \tag{7}$$

Here '$\gtrapprox$' omits negligible rounding errors.

Corollary 3.2 depicts an extreme case in which the majority of signals are swamped, causing the corresponding states to remain seemingly constant. The following example, based on synthetic data, provides further empirical evidence without the fixed Δ_t condition.

Example 3.3 (Synthetic uniform signals). Consider $X \in \mathbb{R}^{1000}$, where both the initial states and subsequent received signals are independently drawn from a uniform distribution $\mathcal{U}[0,1]$. Figure 2 depicts the converged state values after 100 iterations.

It is evident that both linear and dynamic exponent quantization fail to converge to the expected value of 0.5 for a slightly large tensor when the momentum parameter $\beta \to 1$ is adopted. This also explains why the previous approaches (Dettmers et al., 2022; Li et al., 2023a) relied heavily on block-wise quantization. In contrast, the solution proposed below exhibits exceptional robustness, making it more suitable for the unsigned EMA update.

3.2.2. Our Unsigned EMA State Quantization

Stochastic rounding. The swamping problem would not exist any more if we apply *stochastic rounding* (Xia et al., 2020) instead of the nearest rounding method used in the Eq. (1). Without loss of generality, for a $y_{k-1} \leq x/\Delta \leq y_k$, stochastic rounding suggests

$$Q_{sr}(x) := \begin{cases} k-1 & w.p. \ \frac{y_k - x/\Delta}{y_k - y_{k-1}}, \\ k & w.p. \ \frac{x/\Delta - y_{k-1}}{y_k - y_{k-1}}. \end{cases} \tag{8}$$

As a result, even receiving a very small signal z_{t+1}, it could benefit from a non-zero probability, thereby escaping from the swamped state. Unfortunately, this is often accompanied by high variance when quantizing a state value close to zero, as the unsigned EMA state typically appears in the denominator. To be specific, the stochastic rounding in Eq. (8) demonstrates a variance as follows:

Proposition 3.4. *For a 2nd state value $y_{k-1} \leq x/\Delta \leq y_k$ to be quantized, the corresponding adaptive learning rate has a variance:*

$$\mathbf{Var}\left(\frac{1}{\sqrt{\hat{x}}}\right) = \mathcal{O}\left(\left(\frac{\Delta}{\sqrt{y_k}} - \frac{\Delta}{\sqrt{y_{k-1}}}\right)^2\right). \tag{9}$$

As observed, with the same spacing $|y_k - y_{k-1}|$, a higher variance is likely to arise as the value $y_{k-1} \to 0$ from the right. To mitigate this issue, more quantization levels should be allocated near the zero point to provide compensation. This justifies that the commonly used linear or dynamic exponent quantization methods may not be well-suited in this scenario, as they fail to adequately account for this consideration.

As shown in Figure 3, we therefore adopt the logarithmic quantization with a specific base $\alpha \in (0,1)$, where the

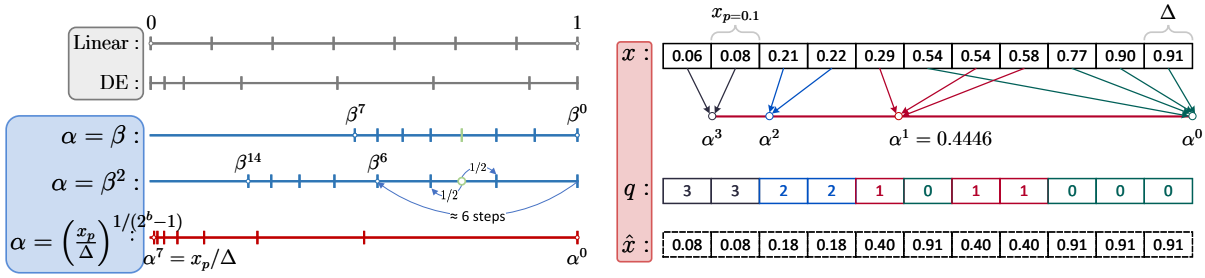

(a) 3-bit quantization levels

(b) 2-bit quantization illustration

Figure 3. (a) Comparison of various quantization approaches: The proposed allocates a greater number of quantization levels near the zero point, effectively reducing variance. (b) Illustration of 2-bit unsigned quantization: 2-digit precision number is shown for clarity.

levels[1] become $y_k = \alpha^k,\ k = 0, \ldots, 2^b - 1$. In addition, we apply a rounding mechanism slightly different to Eq. (8):

$$Q(x) = \text{Clip}(\lfloor \log_\alpha \frac{x}{\Delta} + \xi \rceil; 0, 2^b - 1) \approx \underset{k=0}{\overset{2^b-1}{\text{argmin}}} \left| \frac{x}{\Delta} \cdot \alpha^\xi - y_k \right|, \tag{10}$$

where $\xi \sim \mathcal{U}[-0.5, 0.5]$ and $\lfloor \cdot \rceil$ denotes the convergent rounding used in IEEE 754 floating-point operations. This stochastic rounding mechanism is preferred here because 1) It is straightforward to implement, as it eliminates the need to calculate an level-specific probability for each state value; 2) It allows for a exact exponential decay when consecutive zero signals are received, aligning with the real state decay:

Proposition 3.5 (Consecutive zero signals)**.** *For a state value starts with β^{ck}, $c, k \in \mathbb{N}_+$, it takes $c \cdot s$ iterations to decay to $(\beta^c)^{k+s}$ if the subsequent signals $z \equiv 0$. For the logarithmic quantization with a base $\alpha = \beta^c$, the average number of iterations required to decay from $(\beta^c)^k$ to $(\beta^c)^{k+s}$ is given by*

$$\mathbb{E}\left[(\beta^c)^k \xrightarrow{\textit{Ours}} (\beta^c)^{k+s} \middle| z \equiv 0\right] = cs, \tag{11}$$

which aligns with the the real state decay.

It is worth noting that aligning this state decay is of particular value if parameters are partially involved during training. This situation is frequently encountered during the construction of massive embedding tables, which serve as fundamental components in both natural language processing and recommender systems. Because only a subset of embeddings is sampled during each mini-batch training iteration, the resulting gradient tends to be highly sparse. In addition, some operations such as dropout can also result in zero gradients.

[1]Notably, unlike the convention, the levels here are arranged in a monotonically decreasing order for the sake of notational simplicity. Nevertheless, the aforementioned conclusions remain valid and applicable.

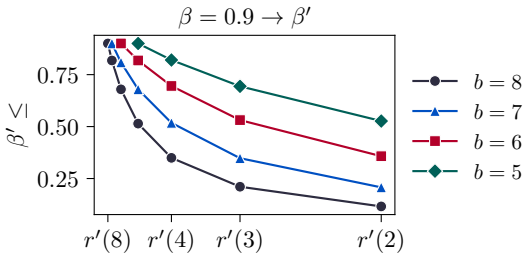

	$b = 8$	$b = 7$	$b = 6$	$b = 5$
$b' = 4$	0.350	0.518	0.695	0.820
$b' = 3$	0.211	0.348	0.531	0.694
$b' = 2$	0.116	0.207	0.357	0.527

Figure 4. The upper bound of β' for DE according to Eq. (15).

The interval $[x_{\min}, \Delta]$ could be fully covered with both endpoints being exactly achievable, if $\alpha = (x_{\min}/\Delta)^{1/(2^b-1)}$. However, the minimum value $x_{\min}$ is numerically unstable and may potentially act as an outlier, especially for a tensor of large size. Therefore, the final desired base is defined as $\alpha = (x_p/\Delta)^{1/(2^b-1)}$ with x_p being the p-quantile of the entire tensor to be quantized. Empirically, a value of $p \in [0.05, 0.3]$ has been found to be effective across various scenarios from small to giant models. Figure 3b illustrates a toy example of 2-bit unsigned logarithmic quantization.

3.3. Quantization for Signed EMA Update

As discussed earlier, the signed EMA state quantization is only minimally impacted by the signal swamping problem due to its signed nature and typically small momentum value β. Nonetheless, it presents two distinct challenges in

comparison to unsigned EMA state quantization:

- Signed quantization must allocate one bit to represent the sign, which inevitably amplifies quantization errors under the same precision constraint.
- The signed state demonstrates significantly higher sensitivity to quantization errors. A substantial quantization error could potentially reverse the descent direction to an ascent direction, significantly impairing convergence.

As a result, training failures are frequently observed in low-precision quantization, particularly in cases where training begins from scratch. To summarize,

> The signed EMA update, in particular for training from scratch, is highly susceptible to quantization errors due to the additional burden of sign representation and its direct impact on the update direction.

Quantization errors amplify the variance of gradients. Here, we theoretically justify why the signed EMA update is susceptible to quantization errors. Firstly note that the received signal $z = g$ for signed EMA updates represents the *stochastic* gradient over a mini-batch. Some prior studies (Li et al., 2023b; Wang et al., 2024) have demonstrated that reducing gradient variance contributes to the convergence. However, the quantization error can be treated as a component of gradient stochasticity, indeed increasing the variance of gradients.

Theorem 3.6. *Let the maximum radius under b-bit stochastic quantization be*

$$r_{\max}(b) = \max_{k=1}^{2^b-1} \frac{1}{2}|y_k - y_{k-1}|.$$

The quantized EMA state update of the stochastic gradient g is equivalent to a standard EMA state update:

$$x_{t+1} \leftarrow \beta \cdot x_t + (1-\beta) \cdot \tilde{g}_{t+1}, \tag{12}$$

where $\tilde{g}_{t+1}$ denotes the stochastic gradient with

$$\mathbb{E}[\tilde{g}_{t+1}] = \mathbb{E}[g_{t+1}], \tag{13}$$

$$\mathbf{Var}[\tilde{g}_{t+1}] \lessapprox \mathbf{Var}[g_{t+1}] + \left(\frac{\beta}{1-\beta} r_{\max}(b) \cdot \Delta_t\right)^2. \tag{14}$$

Theorem 3.6 suggests that as the spacing between the quantization levels decreases or the momentum hyperparameter β increases, the additional gradient variance is progressively introduced. The former implies that the high gradient variance is almost inevitable in the ultra-low-bit scenario, where large spacing arises due to the insufficient number of levels. Clearly, the breakthrough here does not lie in the design of a quantization scheme. SOLO thus turns to a modified momentum hyperparameter β' to regulate the variance introduced by quantization within an acceptable range. If the model converges properly under b-bit quantization with a momentum hyperparameter β, we hypothesize that a similar convergence rate can be achieved with a modified combination of (β', b') subject to

$$\frac{\beta'}{1-\beta'} r_{\text{median}}(b') \leq \frac{\beta}{1-\beta} r_{\text{median}}(b). \tag{15}$$

It is worth noting that r_{median} is adopted in place of $r_{\max}$ because the ratio of $r_*(b)/r_*(b')$ is nearly identical for both the median and maximum radius while the former demonstrates greater stability under ultra-low-bit cases. Figure 4 illustrates the β' allowed for unsigned DE quantization. Empirically, 5-bit quantization is sufficient to maintain accuracy in most fine-tuning scenarios; hence, we adopt the corresponding β' in $b = 4, 3, 2$ bits as an alternative to $\beta = 0.9$. Nevertheless, the optimal β' should be determined based on practical scenarios. For example, training from scratch is more susceptible to quantization errors in comparison to fine-tuning, and thus a lower β' corresponding to 8-bit should be considered.

3.4. Application: 4/2-bit and 2-bit Adam(W)

Since Adam(W) (Kingma & Ba, 2015; Loshchilov & Hutter, 2017) is the most widely adopted optimizer for training and fine-tuning, we introduce in detail two SOLO-quantized variants of Adam(W).

- **4/2-bit Adam(W)** applys a 4-bit DE quantization to the signed EMA update, while a 2-bit logarithmic quantization, as introduced in Eq. (10), to the unsigned EMA update. Notably, it yields memory savings equivalent to a 3-bit Adam(W) while offering additional advantages: 1) As previously discussed, the signed EMA update is more susceptible to quantization errors and should therefore be allocated more bits if possible; 2) Technically, until the work done, mainstream deep learning frameworks have only provided official low-bit storage up to 8-bit precision. To this end, two 4-bit entries or four 2-bit entries should be packed into a single 8-bit element for storage, whereas such straightforward packing is not feasible for 3-bit representations. In addition, based on Figure 4 and empirical observations, a reduced value of $\beta \leq 0.820$ for fine-tuning and $\beta \leq 0.350$ for training from scratch generally ensures a stable training process. In default, we fix the momentum of the *signed* EMA update at 0.8 for fine-tuning and 0.3 for training from scratch, while keeping the momentum for the *unsigned* EMA update unchanged.
- **2-bit Adam(W)** applies 2-bit quantization to both the signed and unsigned EMA updates, representing the ex-

treme case explored in this study. Note that this implies the 32-bit state values would be quantized into only four levels; the signed state encounters an additional challenge, as one bit must be allocated for sign representation, thereby reducing the effective precision. Analogous to the 4/2-bit Adam(W), unless otherwise specified, we fix the momentum of the *signed* EMA update at 0.5 for fine-tuning and 0.1 for training from scratch, while keeping the momentum of the *unsigned* EMA update unchanged. Regarding the p-quantile used in the tailored logarithmic quantization, we fix $p = 0.1$ for simplicity.

Following previous low-bit optimizers (Dettmers et al., 2022; Li et al., 2023a), block-wise quantization with a block size of 128 is adopted. This approach splits the entire tensor into blocks and performs quantization separately on each block. However, we emphasize that the developed unsigned logarithmic quantization is robust to the choice of block size, whereas this is not the case for other approaches.

4. Experiments

In this section, we aim to investigate the superiority of SOLO by comparing it with its full-precision counterparts as well as other low-bit alternatives.

Tasks. Since low-bit optimizers are model- and task-agnostic techniques, they are expected to be applicable across a wide range of scenarios. Here, we consider three primary application domains, Computer Vision (CV), Natural Language Processing (NLP), and Recommender Systems (RS), to ensure a reliable and comprehensive evaluation. CV and NLP are tasks that attract significant interest from the research community, while RS represents a practical application receiving particular focus from the industrial sector. For each domain, we initially employ some benchmarks that are relatively modest in scale by current standards. In addition, we further investigate the performance of instruction tuning for both Large Language Model (LLM) and Large Vision Model (LVM). Detailed descriptions of the models and datasets are provided in the Appendix C.1.

Baselines. We consider baselines ranging from full-precision to 2-bit optimizers. The 16-bit Adam(W) optimizer is implemented using a standard BF16 format, which has been validated in the large-scale training of DeepSeek-v3 (Liu et al., 2024b). The 8-bit Adam(W) variant (Dettmers et al., 2022) employs the dynamic exponent quantization for both signed and unsigned cases. For the lower-precision 4-bit and 2-bit counterparts, as suggested by (Li et al., 2023a), a modified linear quantization scheme that excludes the zero point is employed for unsigned quantization while keeping the signed dynamic exponent quantization unchanged. For a fair comparison, SOLO and other low-bit counterparts adopt block-wise quantization with a size of 128. However, as demonstrated in Figure 5, this constraint can be significantly relaxed for SOLO, whereas other approaches are highly sensitive to it.

Implementation details. We implement SOLO-quantized and other low-bit optimizers based on the same PyTorch-based library, torchao[2]. Training and fine-tuning protocols strictly follow the official codebase, with the only exception being a modified batch size to accommodate the available GPUs. Most of the results reported below are averaged over three independent runs. Given the robust performance and high computational demands of Swin-T and LLaVA-1.5, we limit our evaluation to a single run. The specific hyperparameter settings are listed in Appendix C.1.

4.1. Overall Comparison

In Table 1 and 2, we compare SOLO-quantized 4/2-bit Adam(W) and 2-bit Adam(W) with other low-precision counterparts, covering diverse models, tasks, and training strategies. There are some promising observations:

- Through the comparisons presented in Table 1, particularly the results obtained by training from scratch (🔥), it is evident that the original full-precision (*i.e.*, 32-bit) states contain considerable redundancy, allowing a straightforward reduction in precision to 8-bit format. However, this redundancy alone is insufficient to support further reductions to 4, 3, or 2 bits without addressing the aforementioned challenges, resulting in potential training instability or even training failure. Remark that in the original paper (Li et al., 2023a), the 4-bit Adam(W) optimizer achieves competitive performance on the Swin-T training task. The discrepancy may arise from our adoption of a stricter unified block-wise quantization strategy (tensors containing less than 4096 entries are quantized as well) to ensure a fair comparison. Owing to the attention to signal swamping and high variance, SOLO-quantized optimizers are able to achieve comparable performance even in the extreme case of 2-bit quantization.
- LLM fine-tuning demonstrates a surprising tolerance to quantization errors: no training collapses are observed, and the resulting performance consistently surpasses that of the original base model. However, 8-, 4-, and 2-bit optimizers quantized by previous strategies evidently converge to local optima, making it difficult to believe that they can replace the full-precision AdamW optimizer. The proposed SOLO quantization scheme substantially mitigates this issue, owing to its specific considerations of signal swamping and high gradient variance challenges. The 4/2-bit variant outperforms most low-precision counterparts, with performance on three out of five benchmarks even exceeding that of the half-precision (*i.e.*, 16-bit)

[2] https://github.com/pytorch/ao

		Swin-T 🔥 ImageNet-1K		Transformer-B 🔥 WMT	RoBERTa-L 🔥 GLUE	DCN 🔥 Criteo		HSTU-L 🔥 ML-1M	
		ACC@1	ACC@5	BLEU	ACC/Corr	AUC	LOGLOSS↓	HR	NDCG
	32-bit Adam(W)	81.16	95.55	27.45	88.51	81.38	0.43812	32.73	18.80
	16-bit Adam(W)	80.73	95.29	27.37	88.72	81.06	0.44111	32.83	18.82
	8-bit Adam(W)	80.75	95.43	27.50	88.56	81.35	0.43833	32.70	18.65
	4-bit Adam(W)	Crash	Crash	26.93	88.55	81.00	0.44182	32.75	18.50
	2-bit Adam(W)	Crash	Crash	Crash	88.31	79.10	0.45867	31.39	17.66
SOLO	4/2-bit Adam(W)	80.86	95.48	27.31	88.59	81.36	0.43825	32.57	18.52
SOLO	2-bit Adam(W)	80.74	95.39	27.12	88.66	81.32	0.43861	32.03	18.20

(a) CV (b) NLP (c) RS

Table 1. The performance of low-bit optimizers in (a) Computer Vision (CV); (b) Natural Language Processing (NLP); (c) Recommender System (RS). 🔥: Training from scratch; 🔥: Fine-tuning; Crash: A training failure is encountered.

		LLaMA-7B 🔥						
		MMLU	ARC-e	ARC-c	OBQA	SIQA	Memory	Time
	Pretrained	35.34	48.85	43.39	29.40	44.58		
	32-bit AdamW	40.80	60.61	47.01	43.80	48.50	50.24GB	8.7h
	16-bit AdamW	40.94	58.73	47.23	41.40	48.21	25.12GB	8.9h
	8-bit AdamW	40.34	59.49	44.52	42.20	48.05	12.97GB	9.3h
	4-bit AdamW	40.58	59.20	45.76	42.41	48.94	6.69GB	9.1h
	2-bit AdamW	39.84	57.26	45.09	39.53	47.31	3.41GB	9.0h
SOLO	4/2-bit AdamW	41.03	60.08	46.44	43.07	47.88	5.18GB	9.1h
SOLO	2-bit AdamW	40.36	59.85	45.88	40.47	47.21	3.61GB	9.1h

(a) LLM (Large Language Model). The Wilcoxon signed-rank test (two-tailed) between the SOLO-quantized 4/2-bit AdamW optimizer and its full 32-bit counterpart indicates a p-vlue of 0.125, namely no statistically significant difference in performance.

		LLaVA-1.5 🔥					
		ScienceQA	TextVQA	POPE	MME	Memory	Time
	32-bit AdamW	70.81	58.50	72.40	1485.53	50.49GB	22.95h
	16-bit AdamW	71.30	58.04	72.61	1451.10	25.25GB	22.70h
	8-bit AdamW	70.62	57.98	72.79	1463.13	13.05GB	25.59h
	4-bit AdamW	70.69	58.62	73.01	1439.57	6.76GB	24.39h
	2-bit AdamW	28.93	54.10	72.57	1417.93	3.61GB	23.87h
SOLO	4/2-bit AdamW	70.81	58.10	72.43	1474.91	5.38GB	24.53h
SOLO	2-bit AdamW	69.51	57.76	72.34	1472.77	3.81GB	23.81h

(b) LVM (Large Vision Model). The Wilcoxon signed-rank test (two-tailed) between the SOLO-quantized 4/2-bit AdamW optimizer and its full 32-bit counterpart indicates a p-vlue of 0.285, namely no statistically significant difference in performance.

Table 2. The comparison of low-bit optimizers in giant model fine-tuning. (a) LLaMA-7B instruction tuning; (b) LLaVA-1.5 visual instruction tuning based on Vicuna-7B-v1.5. 'Memory': The memory storage required for the optimizer; 'Time': The total training time (in hours).

Q	Block size: 128					Block size: 2048				
	MMLU	ARC-e	ARC-c	OBQA	SIQA	MMLU	ARC-e	ARC-c	OBQA	SIQA
DE	0.00	0.00	0.00	0.00	32.91	0.00	0.00	0.00	0.00	32.91
Linear	40.82	57.73	46.67	40.60	47.39	38.46	53.56	44.07	36.07	45.34
Ours	41.03	60.08	46.44	43.07	47.88	40.63	58.20	46.67	41.07	48.36

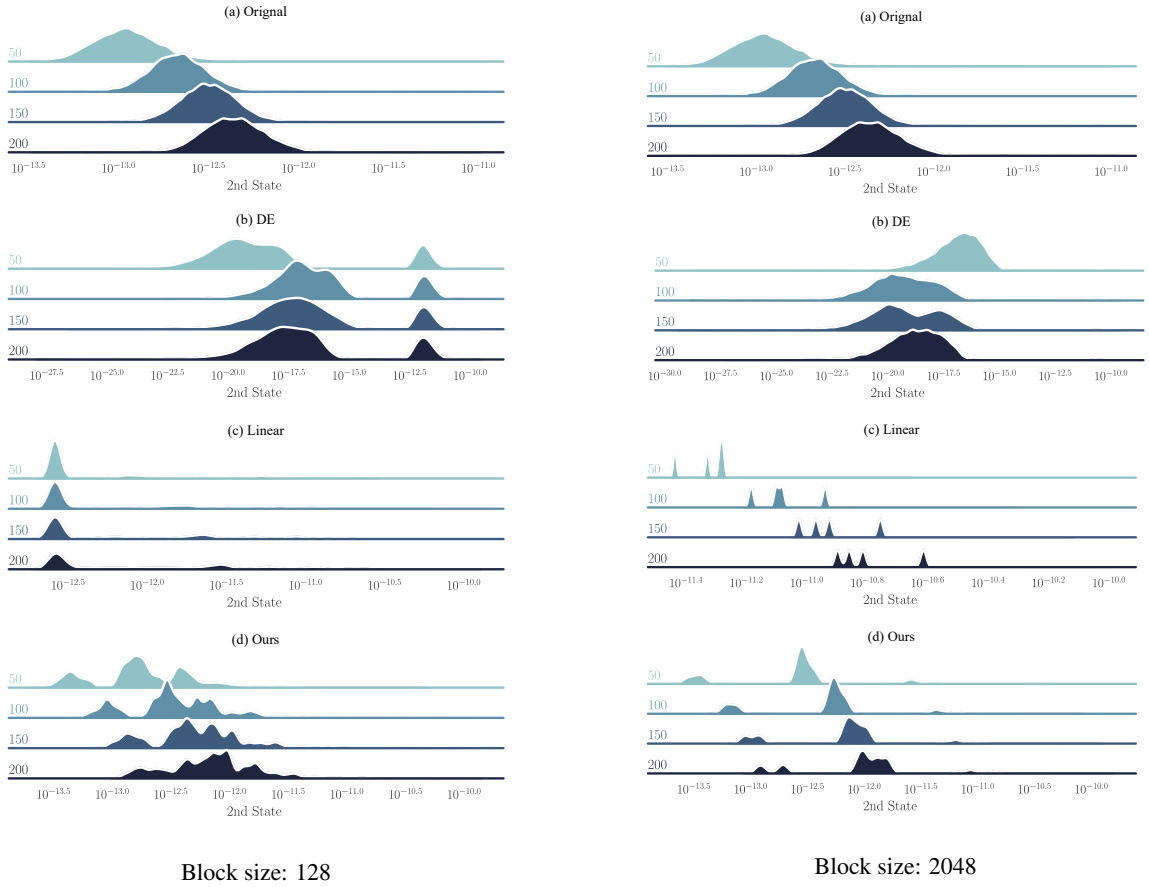

Figure 5. Block size generalizability. The top panel reports the results fine-tuned with a 4/2-bit AdamW whose 2nd EMA update is quantized by DE, Linear (excluding the zero point), and the tailored logarithmic quantization. The bottom panel illustrates how the 2nd state distribution over partial weights changes at steps 50, 100, 150, and 200.

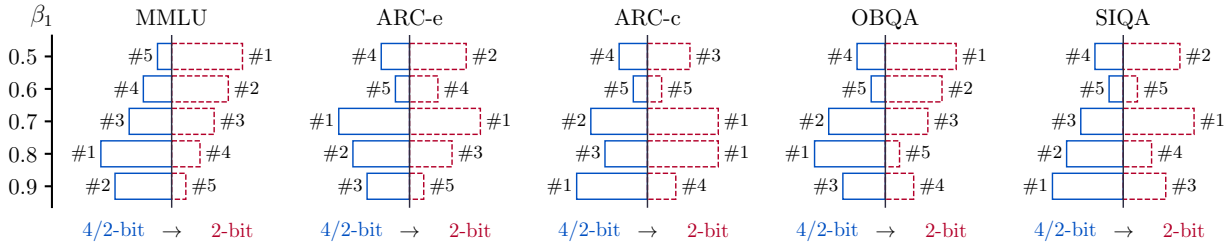

Figure 6. The necessity of reducing β_1 when ultra-low-bit quantization is applied to the 1st states. '#' indicates the rank (lower is better) among fine-tuned models of varying β_1 (from 0.5 to 0.9).

AdamW optimizer. Admittedly, fine-tuning with the 2-bit configuration remains highly challenging for large-scale fine-tuning; nonetheless, it still attains performance comparable to that of the 8-bit AdamW optimizer.

- For visual instruction tuning, the performance degradation caused by quantization errors is negligible until 2-bit representation. This is because the MLP projector that bridges the visual encoder tower (CLIP) and the LLM (Vicuna-7B-v1.5) has already been pretrained in full precision. However, scaling to a fully 2-bit setting remains a significant challenge. Thanks to SOLO's gradient variance control, the 2-bit quantized AdamW optimizer under SOLO still exhibits competitive performance. It is worth noting that, in some cases, the ultra-low-bit optimizer even outperforms its full-precision counterpart. This phenomenon can be attributed to the fact (Zhang et al., 2024b) that grouping elements within a block to share the same adaptive learning rate (*i.e.*, the 2nd moment) may facilitate a better convergence.

- Note that low-bit optimizers typically incur additional computational overhead, resulting in slightly longer training times. Nonetheless, this overhead could be further reduced by optimizing our implementation with fused operators, as suggested by (Li et al., 2023a). However, the implementation of the specified fused operators demands technical engineering effort, which lies beyond the scope of this work and is left for future work.

4.2. Generalizability

- **Block size.** Block-wise quantization has been widely adopted to narrow the numerical range subject to quantization, thereby significantly reducing quantization errors. However, the block size cannot be indefinitely reduced, as each 32-bit scale factor Δ introduces an additional overhead of $1/4$ bits per block. In the case of SOLO, the presence of a buffered logarithmic base incurs the double overhead, amounting to $1/2$ bits per block. Consequently, a block size of 128 is approximately the smallest permissible. Nonetheless, we argue that the proposed logarithmic quantization has remarkable generalizability in this aspect. Figure 5 compares the results under block sizes of 128 and 2048, where our method significantly outperforms the others. The bottom panel further substantiates the superiority of our approach, as the proposed logarithmic quantization preserves state dynamics that closely resemble those of the original 32-bit AdamW.

- **AdaBelief.** Although the results in Table 1 involve the Adam and AdamW optimizers, it is of interest to examine the generalizability of SOLO to other optimizers that incorporate an EMA update mechanism. Table 3 presents the application of SOLO to AdaBelief (Zhuang et al., 2020), which also demonstrates comparable performance.

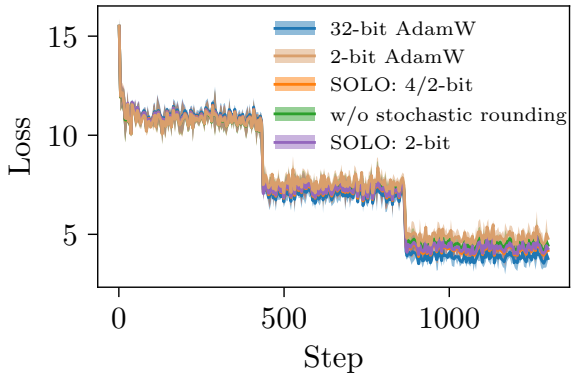

Figure 7. The training loss on LLaMA fine-tuning.

Remark that SOLO can also be applied to lightweight optimizers such as Adafactor (Shazeer & Stern, 2018). However, the use of FSDP renders the comparison infeasible, as the optimizer states in this case are flattened and partitioned, making the row-wise and column-wise states maintained in Adafactor invalid.

AdaBelief	MMLU	ARC-e	ARC-c	OBQA	SIQA
32-bit	40.78	59.55	44.63	42.73	47.80
4/2-bit	40.39	58.96	45.88	42.47	47.94

Table 3. Application of SOLO to AdaBelief.

4.3. Empirical Analysis

Some empirical analysis is performed in this part to provide intuitive exposition of SOLO.

- **Modified β_1.** We discuss in Section 3.3 the necessity of reducing β_1 to regulate the gradient variance introduced by quantization. As shown in Figure 6, the LLaMA model fine-tuned with 4/2-bit AdamW performs optimally at $\beta_1 = 0.8$ or 0.9, and its performance deteriorates as β_1 decreases. Conversely, the performance of the model improves in the 2-bit case and reaches its best near $\beta_1 = 0.5$. This confirms our theoretical findings and the rationale summarized in Figure 4.

- **Loss curve.** As illustrated in Figure 7, the SOLO-quantized 4/2-bit and 2-bit AdamW optimizers demonstrate loss curves closely resembling that of the original full-precision AdamW. In contrast, the 2-bit AdamW that incorporates the quantization approaches proposed in (Li et al., 2023a) exhibits significantly poorer convergence, consequently resulting in consistently inferior performance. In addition, the specialized rounding mechanism introduced in Eq. (10) is essential; otherwise, a deteriorated loss curve would be observed.

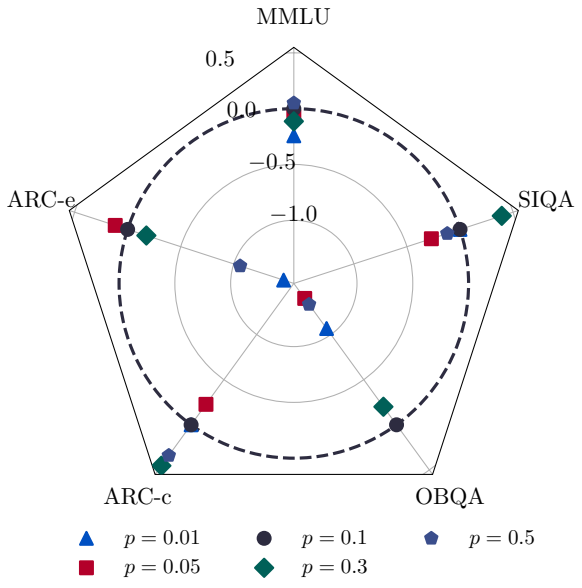

Figure 8. Sensitivity analysis of p-quantile. For clarity, we illustrate the differences relative to the default value of $p = 0.1$.

- **Logarithmic base.** Figure 8 demonstrates how sensitive of SOLO to the choice of logarithmic base α. Recall that $\alpha = (x_p/\Delta)^{1/(2^b-1)}$ is determined by the p-quantile x_p. When p is too large (*i.e.*, $p \to 1$), more small state values are directly truncated, leading to high-variance learning rates. Conversely, when p is too small (*i.e.*, $p \to 0$), the base choice tends to be an outlier, resulting in unacceptable quantization errors. Fortunately, SOLO exhibits a satisfactory robustness as $p \in [0.05, 0.3]$.

5. Conclusion

SOLO is designed to slim down the most memory-intensive component during training, guided by two key principles: (I) Generalizability. Although certain optimizers are lightweight by design, their generalizability has not been thoroughly validated compared to the widely adopted Adam(W) optimizer. SOLO is a model-, task-, and hardware-independent technique, as it is capable of keeping consistent optimization dynamics even after ultra-low-bit quantization. (II) Flexibility. The application of certain distributed algorithms and network quantization approaches demands substantial engineering effort. On the contrary, SOLO can be seamlessly applied to most Adam-style optimizers without the need to retune hyperparameters such as the learning rate or weight decay.

Previous efforts have achieved certain success in 8-bit or 4-bit quantization; however, they violate the generalizability principle. On the one hand, they overlook the signal swamping problem frequently arised in unsigned EMA updates, leading to poor approximation to the true state dynamics. In other words, their application essentially changes the nature of the original optimizer in the ultra-low-bit case, thereby failing to guarantee that performance is maintained. On the other hand, signed quantization approaches can not be directly scaled to ultra-low precision owing to the increased gradient variance; otherwise, training failures are likely to occur. SOLO addresses these two challenges through comprehensive theoretical analysis, adhering to the principles of both generalizability and flexibility.

The limitations of SOLO motivate future research on how to further unleash the potential of ultra-low-bit signed quantization in large-scale model training. According to the analysis in this paper, the signed EMA update is highly susceptible to the quantization errors due to the additional burden of sign representation and its direct impact on the update direction. Recent advances in sign gradient descent (Chen et al., 2024) may offer particular advantages in addressing this issue. Finally, although the superiority of SOLO has been demonstrated across various domains and training protocols, its effectiveness in large-scale model (*e.g.*, 175B) pretraining remains unverified due to prohibitive computational costs. Conducting such an extensive evaluation would require the resources of a large AI research organization, which is beyond the scope of this study.

The prosperity of AI stems from the collective efforts of individual researchers within the community; however, the rapid scaling of model sizes is rendering fundamental research accessible only to those equipped with substantial computational infrastructure. There is an urgent need for affordable alternatives to reinvigorate research interest. SOLO advances this goal by slimming down the optimizer, which is the most memory-intensive part of the training process.

References

Anil, R., Gupta, V., Koren, T., and Singer, Y. Memory efficient adaptive optimization. In *Advances in Neural Information Processing Systems (NeurIPS)*, volume 32, 2019.

Anil, R., Dai, A. M., Firat, O., Johnson, M., Lepikhin, D., Passos, A., Shakeri, S., Taropa, E., Bailey, P., Chen, Z., et al. Palm 2 technical report. *arXiv preprint arXiv:2305.10403*, 2023.

Ashkboos, S., Markov, I., Frantar, E., Zhong, T., Wang, X., Ren, J., Hoefler, T., and Alistarh, D. Towards end-to-end 4-bit inference on generative large language models. In *Conference on Empirical Methods in Natural Language Processing (EMNLP)*, pp. 3355–3371, 2024.

Bai, J., Bai, S., Chu, Y., Cui, Z., Dang, K., Deng, X., Fan,

Y., Ge, W., Han, Y., Huang, F., et al. Qwen technical report. *arXiv preprint arXiv:2309.16609*, 2023.

Caesar, H., Uijlings, J., and Ferrari, V. Coco-stuff: Thing and stuff classes in context. In *IEEE Conference on Computer Vision and Pattern Recognition (CVPR)*, pp. 1209–1218, 2018.

Chen, X., Liang, C., Huang, D., Real, E., Wang, K., Pham, H., Dong, X., Luong, T., Hsieh, C.-J., Lu, Y., et al. Symbolic discovery of optimization algorithms. In *Advances in Neural Information Processing Systems (NeurIPS)*, volume 36, 2024.

Chiang, W.-L., Li, Z., Lin, Z., Sheng, Y., Wu, Z., Zhang, H., Zheng, L., Zhuang, S., Zhuang, Y., Gonzalez, J. E., Stoica, I., and Xing, E. P. Vicuna: An open-source chatbot impressing gpt-4 with 90%* chatgpt quality, March 2023. URL https://lmsys.org/blog/2023-03-30-vicuna/.

Clark, P., Cowhey, I., Etzioni, O., Khot, T., Sabharwal, A., Schoenick, C., and Tafjord, O. Think you have solved question answering? try arc, the ai2 reasoning challenge. *arXiv preprint arXiv:1803.05457*, 2018.

Contributors, O. Opencompass: A universal evaluation platform for foundation models. https://github.com/open-compass/opencompass, 2023.

Deng, J., Dong, W., Socher, R., Li, L.-J., Li, K., and Fei-Fei, L. Imagenet: A large-scale hierarchical image database. In *IEEE Conference on Computer Vision and Pattern Recognition (CVPR)*, pp. 248–255, 2009.

Dettmers, T. 8-bit approximations for parallelism in deep learning. In *International Conference on Learning Representations (ICLR)*, 2015.

Dettmers, T., Lewis, M., Shleifer, S., and Zettlemoyer, L. 8-bit optimizers via block-wise quantization. In *International Conference on Learning Representations (ICLR)*, 2022.

Dosovitskiy, A., Beyer, L., Kolesnikov, A., Weissenborn, D., Zhai, X., Unterthiner, T., Dehghani, M., Minderer, M., Heigold, G., Gelly, S., et al. An image is worth 16x16 words: Transformers for image recognition at scale. In *International Conference on Learning Representations (ICLR)*, 2020.

Frantar, E., Ashkboos, S., Hoefler, T., and Alistarh, D. Gptq: Accurate post-training quantization for generative pre-trained transformers. *arXiv preprint arXiv:2210.17323*, 2022.

Fu, C., Chen, P., Shen, Y., Qin, Y., Zhang, M., Lin, X., Qiu, Z., Lin, W., Yang, J., Zheng, X., Li, K., Sun, X., and Ji, R. MME: A comprehensive evaluation benchmark for multimodal large language models. *CoRR*, abs/2306.13394, 2023.

Gao, C., Chen, J., Zhao, K., Wang, J., and Jing, L. 1-bit fqt: Pushing the limit of fully quantized training to 1-bit. *arXiv preprint arXiv:2408.14267*, 2024.

GenAI, M. Llama 2: Open foundation and fine-tuned chat models. *arXiv preprint arXiv:2307.09288*, 2023.

Gu, A. and Dao, T. Mamba: Linear-time sequence modeling with selective state spaces. *arXiv preprint arXiv:2312.00752*, 2023.

Han, Z., Gao, C., Liu, J., Zhang, J., and Zhang, S. Q. Parameter-efficient fine-tuning for large models: A comprehensive survey. *arXiv preprint arXiv:2403.14608*, 2024.

Hendrycks, D., Burns, C., Basart, S., Zou, A., Mazeika, M., Song, D., and Steinhardt, J. Measuring massive multitask language understanding. *arXiv preprint arXiv:2009.03300*, 2020.

Higham, N. J. The accuracy of floating point summation. *SIAM Journal on Scientific Computing*, 14(4):783–799, 1993.

Hu, E. J., Shen, Y., Wallis, P., Allen-Zhu, Z., Li, Y., Wang, S., Wang, L., and Chen, W. Lora: Low-rank adaptation of large language models. In *International Conference on Learning Representations (ICLR)*, 2021.

Hudson, D. A. and Manning, C. D. Gqa: A new dataset for real-world visual reasoning and compositional question answering. In *IEEE Conference on Computer Vision and Pattern Recognition (CVPR)*, pp. 6700–6709, 2019.

Katharopoulos, A., Vyas, A., Pappas, N., and Fleuret, F. Transformers are rnns: Fast autoregressive transformers with linear attention. In *International Conference on Machine Learning (ICML)*, pp. 5156–5165. PMLR, 2020.

Kingma, D. P. and Ba, J. Adam: A method for stochastic optimization. In *International Conference on Learning Representations (ICLR)*, 2015.

Krishna, R., Zhu, Y., Groth, O., Johnson, J., Hata, K., Kravitz, J., Chen, S., Kalantidis, Y., Li, L.-J., Shamma, D. A., et al. Visual genome: Connecting language and vision using crowdsourced dense image annotations. *International journal of computer vision*, 123:32–73, 2017.

Li, B., Chen, J., and Zhu, J. Memory efficient optimizers with 4-bit states. In *Advances in Neural Information Processing Systems (NeurIPS)*, 2023a.

Li, H., Rakhlin, A., and Jadbabaie, A. Convergence of adam under relaxed assumptions. In *Advances in Neural Information Processing Systems*, volume 36, pp. 52166–52196, 2023b.

Li, X. L. and Liang, P. Prefix-tuning: Optimizing continuous prompts for generation. In *Annual Meeting of the Association for Computational Linguistics (ACL)*, pp. 4582–4597, 2021.

Li, Y., Du, Y., Zhou, K., Wang, J., Zhao, W. X., and Wen, J.-R. Evaluating object hallucination in large vision-language models. In *Conference on Empirical Methods in Natural Language Processing (EMNLP)*, pp. 292–305, 2023c.

Lin, H., Xu, H., Wu, Y., Cui, J., Zhang, Y., Mou, L., Song, L., Sun, Z., and Wei, Y. Duquant: Distributing outliers via dual transformation makes stronger quantized llms. In *Advances in Neural Information Processing Systems (NeurIPS)*, volume 37, pp. 87766–87800, 2025.

Lin, J., Tang, J., Tang, H., Yang, S., Chen, W.-M., Wang, W.-C., Xiao, G., Dang, X., Gan, C., and Han, S. Awq: Activation-aware weight quantization for on-device llm compression and acceleration. In *Conference on Machine Learning and Systems (MLSys)*, volume 6, pp. 87–100, 2024.

Liu, A., Feng, B., Wang, B., Wang, B., Liu, B., Zhao, C., Dengr, C., Ruan, C., Dai, D., Guo, D., et al. Deepseek-v2: A strong, economical, and efficient mixture-of-experts language model. *arXiv preprint arXiv:2405.04434*, 2024a.

Liu, A., Feng, B., Xue, B., Wang, B., Wu, B., Lu, C., Zhao, C., Deng, C., Zhang, C., Ruan, C., et al. Deepseek-v3 technical report. *arXiv preprint arXiv:2412.19437*, 2024b.

Liu, H., Li, C., Wu, Q., and Lee, Y. J. Visual instruction tuning. In *Advances in Neural Information Processing Systems (NeurIPS)*, 2023.

Liu, Y. Roberta: A robustly optimized bert pretraining approach. *arXiv preprint arXiv:1907.11692*, 364, 2019.

Liu, Z., Lin, Y., Cao, Y., Hu, H., Wei, Y., Zhang, Z., Lin, S., and Guo, B. Swin transformer: Hierarchical vision transformer using shifted windows. In *IEEE International Conference on Computer Vision (ICCV)*, pp. 10012–10022, 2021.

Loshchilov, I. and Hutter, F. Decoupled weight decay regularization. In *International Conference on Learning Representations (ICLR)*, 2017.

Lu, P., Mishra, S., Xia, T., Qiu, L., Chang, K.-W., Zhu, S.-C., Tafjord, O., Clark, P., and Kalyan, A. Learn to explain: Multimodal reasoning via thought chains for science question answering. In *Advances in Neural Information Processing Systems (NeurIPS)*, volume 35, pp. 2507–2521, 2022.

Luo, Q., Yu, H., and Li, X. Badam: A memory efficient full parameter optimization method for large language models. In *Advances in Neural Information Processing Systems (NeurIPS)*, volume 37, pp. 24926–24958, 2024.

Micikevicius, P., Narang, S., Alben, J., Diamos, G., Elsen, E., Garcia, D., Ginsburg, B., Houston, M., Kuchaiev, O., Venkatesh, G., et al. Mixed precision training. In *International Conference on Learning Representations (ICLR)*, 2018.

Mihaylov, T., Clark, P., Khot, T., and Sabharwal, A. Can a suit of armor conduct electricity? a new dataset for open book question answering. *arXiv preprint arXiv:1809.02789*, 2018.

Mishra, A., Shekhar, S., Singh, A. K., and Chakraborty, A. Ocr-vqa: Visual question answering by reading text in images. In *International Conference on Document Analysis and Recognition (ICDAR)*, pp. 947–952, 2019.

Oh, S., Sim, H., Lee, S., and Lee, J. Automated log-scale quantization for low-cost deep neural networks. In *Proceedings of the IEEE/CVF Conference on Computer Vision and Pattern Recognition*, pp. 742–751, 2021.

Ott, M., Edunov, S., Grangier, D., and Auli, M. Scaling neural machine translation. *arXiv preprint arXiv:1806.00187*, 2018.

Papineni, K., Roukos, S., Ward, T., and Zhu, W.-J. Bleu: a method for automatic evaluation of machine translation. In *Annual Meeting of the Association for Computational Linguistics (ACL)*, pp. 311–318, 2002.

Radford, A. Improving language understanding by generative pre-training. 2018.

Rajbhandari, S., Rasley, J., Ruwase, O., and He, Y. Zero: Memory optimizations toward training trillion parameter models. In *International Conference for High Performance Computing, Networking, Storage and Analysis*, pp. 1–16. IEEE, 2020.

Rajbhandari, S., Ruwase, O., Rasley, J., Smith, S., and He, Y. Zero-infinity: Breaking the gpu memory wall for extreme scale deep learning. In *International Conference for High Performance Computing, Networking, Storage and Analysis*, pp. 1–14, 2021.

Ren, J., Rajbhandari, S., Aminabadi, R. Y., Ruwase, O., Yang, S., Zhang, M., Li, D., and He, Y. {Zero-offload}: Democratizing {billion-scale} model training. In *2021 USENIX Annual Technical Conference (USENIX ATC 21)*, pp. 551–564, 2021.

Sap, M., Rashkin, H., Chen, D., LeBras, R., and Choi, Y. Socialiqa: Commonsense reasoning about social interactions. *arXiv preprint arXiv:1904.09728*, 2019.

Seide, F., Fu, H., Droppo, J., Li, G., and Yu, D. 1-bit stochastic gradient descent and its application to data-parallel distributed training of speech dnns. In *Interspeech*, volume 2014, pp. 1058–1062. Singapore, 2014.

Shazeer, N. and Stern, M. Adafactor: Adaptive learning rates with sublinear memory cost. In *International Conference on Machine Learning (ICML)*, pp. 4596–4604. PMLR, 2018.

Shazeer, N., Mirhoseini, A., Maziarz, K., Davis, A., Le, Q., Hinton, G., and Dean, J. Outrageously large neural networks: The sparsely-gated mixture-of-experts layer. In *International Conference on Learning Representations (ICLR)*, 2017.

Singh, A., Natarajan, V., Shah, M., Jiang, Y., Chen, X., Batra, D., Parikh, D., and Rohrbach, M. Towards vqa models that can read. In *IEEE Conference on Computer Vision and Pattern Recognition (CVPR)*, pp. 8317–8326, 2019.

Sun, X., Wang, N., Chen, C.-Y., Ni, J., Agrawal, A., Cui, X., Venkataramani, S., El Maghraoui, K., Srinivasan, V. V., and Gopalakrishnan, K. Ultra-low precision 4-bit training of deep neural networks. In *Advances in Neural Information Processing Systems (NeurIPS)*, volume 33, pp. 1796–1807, 2020.

Tang, H., Zhang, X., Liu, K., Zhu, J., and Kang, Z. Mkq-bert: Quantized bert with 4-bits weights and activations. *arXiv preprint arXiv:2203.13483*, 2022.

Taori, R., Gulrajani, I., Zhang, T., Dubois, Y., Li, X., Guestrin, C., Liang, P., and Hashimoto, T. B. Stanford alpaca: An instruction-following llama model. https://github.com/tatsu-lab/stanford_alpaca, 2023.

Touvron, H., Lavril, T., Izacard, G., Martinet, X., Lachaux, M.-A., Lacroix, T., Rozière, B., Goyal, N., Hambro, E., Azhar, F., et al. Llama: Open and efficient foundation language models. *arXiv preprint arXiv:2302.13971*, 2023.

Wang, A., Singh, A., Michael, J., Hill, F., Levy, O., and Bowman, S. GLUE: A multi-task benchmark and analysis platform for natural language understanding. In *Proceedings of the 2018 EMNLP Workshop BlackboxNLP: Analyzing and Interpreting Neural Networks for NLP*, pp. 353–355, 2018a.

Wang, B., Zhang, H., Meng, Q., Sun, R., Ma, Z.-M., and Chen, W. On the convergence of adam under non-uniform smoothness: Separability from sgdm and beyond. *arXiv preprint arXiv:2403.15146*, 2024.

Wang, G., Qin, H., Jacobs, S. A., Holmes, C., Rajbhandari, S., Ruwase, O., Yan, F., Yang, L., and He, Y. Zero++: Extremely efficient collective communication for giant model training. In *International Conference on Learning Representations (ICLR)*, 2023.

Wang, N., Choi, J., Brand, D., Chen, C.-Y., and Gopalakrishnan, K. Training deep neural networks with 8-bit floating point numbers. In *Advances in neural information processing systems*, volume 31, 2018b.

Wang, R., Fu, B., Fu, G., and Wang, M. Deep & cross network for ad click predictions. In *Proceedings of the ADKDD'17*, pp. 1–7, 2017.

Waswani, A., Shazeer, N., Parmar, N., Uszkoreit, J., Jones, L., Gomez, A., Kaiser, L., and Polosukhin, I. Attention is all you need. In *Advances in Neural Information Processing Systems (NeurIPS)*, 2017.

Xi, H., Li, C., Chen, J., and Zhu, J. Training transformers with 4-bit integers. In *Advances in Neural Information Processing Systems (NeurIPS)*, volume 36, pp. 49146–49168, 2023.

Xi, H., Chen, Y., Zhao, K., Teh, K. J., Chen, J., and Zhu, J. Jetfire: Efficient and accurate transformer pretraining with int8 data flow and per-block quantization. In *International Conference on Machine Learning (ICML)*, 2024.

Xia, L., Anthonissen, M., Hochstenbach, M., and Koren, B. Improved stochastic rounding. *arXiv preprint arXiv:2006.00489*, 2020.

Yang, A., Yang, B., Zhang, B., Hui, B., Zheng, B., Yu, B., Li, C., Liu, D., Huang, F., Wei, H., et al. Qwen2. 5 technical report. *arXiv preprint arXiv:2412.15115*, 2024.

Zhai, J., Liao, L., Liu, X., Wang, Y., Li, R., Cao, X., Gao, L., Gong, Z., Gu, F., He, J., et al. Actions speak louder than words: Trillion-parameter sequential transducers for generative recommendations. In *International Conference on Machine Learning (ICML)*, 2024.

Zhang, B., Luo, L., Chen, Y., Nie, J., Liu, X., Li, S., Zhao, Y., Hao, Y., Yao, Y., Wen, E. D., et al. Wukong: Towards a scaling law for large-scale recommendation. In *International Conference on Machine Learning (ICML)*, pp. 59421–59434, 2024a.

Zhang, Y., Chen, C., Li, Z., Ding, T., Wu, C., Ye, Y., Luo, Z.-Q., and Sun, R. Adam-mini: Use fewer learning rates to gain more. *arXiv preprint arXiv:2406.16793*, 2024b.

Zhao, J., Zhang, Z., Chen, B., Wang, Z., Anandkumar, A., and Tian, Y. Galore: Memory-efficient llm training by gradient low-rank projection. In *International Conference on Machine Learning (ICML)*, 2024a.

Zhao, Y., Lin, C.-Y., Zhu, K., Ye, Z., Chen, L., Zheng, S., Ceze, L., Krishnamurthy, A., Chen, T., and Kasikci, B. Atom: Low-bit quantization for efficient and accurate llm serving. In *Conference on Machine Learning and Systems (MLSys)*, volume 6, pp. 196–209, 2024b.

Zhou, A., Yao, A., Guo, Y., Xu, L., and Chen, Y. Incremental network quantization: Towards lossless cnns with low-precision weights. In *International Conference on Learning Representations (ICLR)*, 2017.

Zhuang, J., Tang, T., Ding, Y., Tatikonda, S., Dvornek, N. C., Papademetris, X., and Duncan, J. S. Adabelief optimizer: Adapting stepsizes by the belief in observed gradients. In Larochelle, H., Ranzato, M., Hadsell, R., Balcan, M., and Lin, H. (eds.), *Advances in Neural Information Processing Systems (NeurIPS)*, 2020.

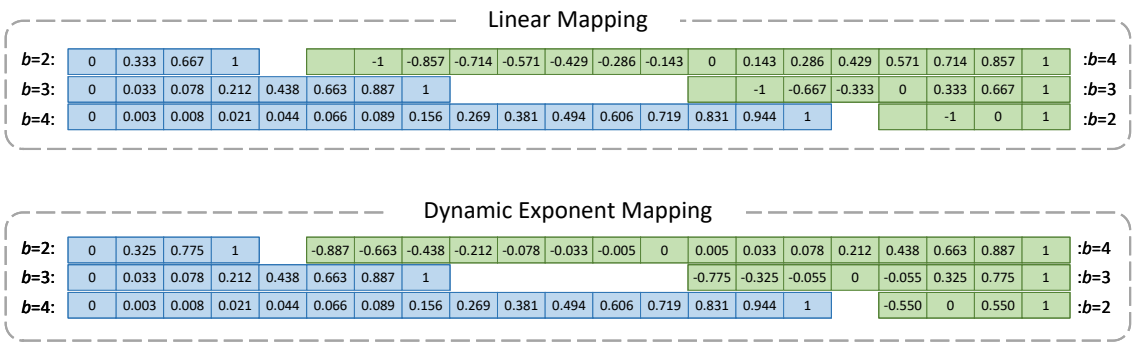

Figure 9. Linear and DE mappings for unsigned and signed cases.

A. Quantization Methods

In this part, we provide a detailed introduction to the aforementioned Linear and Dynamic Exponent (DE) quantization techniques. Particular emphasis is placed on the following mapping formulation, as it effectively unifies the majority of unsigned and signed quantization methods.

$$q = Q(x) := \underset{k=0}{\overset{2^b-1}{\operatorname{argmin}}} \left| \frac{x}{\Delta} - y_k \right|. \tag{16}$$

Linear mapping represents one of the most widely adopted quantization methods due to its straightforward and practical implementation with levels evenly distributed over [0, 1] and [-1, 1]:

$$\text{Unsigned:} \quad \{0, \frac{1}{2^b-1}, \ldots, 1\}; \qquad \text{Signed:} \quad \{0, \pm\frac{1}{2^{b-1}-1}, \ldots, \pm 1\}. \tag{17}$$

The 4-bit Adam developed by Li et al. (2023a) observed a zero-point problem when applying the unsigned linear quantization to 2nd state update, yielding a slightly different variant of $\{\frac{1}{2^b}, \ldots, 1\}$.

Dynamic exponent mapping (Dettmers, 2015) places greater emphasis on handling both small and large magnitude values, as the received signals generally exhibit a non-uniform distribution. In the unsigned case, the b bits are divided to serve three distinct functions:

$$b = \underbrace{E}_{\text{exponent bits}} + \underbrace{1}_{\text{indicator bit}} + \underbrace{F}_{\text{fraction bits}}. \tag{18}$$

The leading zero bits E represents the magnitude of the exponent. The subsequent indicator bit is the first bit set to one, signifying that all remaining bits are allocated for fraction representation. Then, a F-bit linear quantization is performed over the range [0.1, 1]. Naturally, the first bit has to be reserved for the signed case. The 8-bit Adam developed by Dettmers et al. (2022) simplifies this quantization by removing the indicator bit. We illustrate the specific linear and DE mappings across $b = 2, 3, 4$ bits in Figure 9.

Denoted by $r_{\min}, r_{\text{median}}, r_{\max}$ the minimum, median, and maximum over all radii, it is easy to obtain the following fact:

Fact A.1. *The maximum radius:*

- *Linear:*

$$\textit{Unsigned:} \quad r_{\min} = r_{\textit{median}} = r_{\max} \approx \underbrace{0.002}_{\textit{8-bit}}, \underbrace{0.033}_{\textit{4-bit}}, \underbrace{0.071}_{\textit{3-bit}}, \underbrace{0.167}_{\textit{2-bit}};$$

$$\textit{Signed:} \quad r_{\min} = r_{\textit{median}} = r_{\max} \approx \underbrace{0.004}_{\textit{8-bit}}, \underbrace{0.071}_{\textit{4-bit}}, \underbrace{0.167}_{\textit{3-bit}}, \underbrace{0.500}_{\textit{2-bit}}.$$

- *DE:*

$$\textit{Unsigned:}\quad r_{\min} \approx \underbrace{0.000}_{\textit{8-bit}}, \underbrace{0.002}_{\textit{4-bit}}, \underbrace{0.016}_{\textit{3-bit}}, \underbrace{0.113}_{\textit{2-bit}},\ r_{\textit{median}} \approx \underbrace{0.002}_{\textit{8-bit}}, \underbrace{0.034}_{\textit{4-bit}}, \underbrace{0.067}_{\textit{3-bit}}, \underbrace{0.163}_{\textit{2-bit}},$$
$$r_{\max} \approx \underbrace{0.004}_{\textit{8-bit}}, \underbrace{0.056}_{\textit{4-bit}}, \underbrace{0.113}_{\textit{3-bit}}, \underbrace{0.225}_{\textit{2-bit}};$$
$$\textit{Signed:}\quad r_{\min} \approx \underbrace{0.000}_{\textit{8-bit}}, \underbrace{0.003}_{\textit{4-bit}}, \underbrace{0.028}_{\textit{3-bit}}, \underbrace{0.225}_{\textit{2-bit}},\ r_{\textit{median}} \approx \underbrace{0.004}_{\textit{8-bit}}, \underbrace{0.008}_{\textit{7-bit}}, \underbrace{0.017}_{\textit{6-bit}}, \underbrace{0.034}_{\textit{5-bit}}, \underbrace{0.067}_{\textit{4-bit}}, \underbrace{0.135}_{\textit{3-bit}}, \underbrace{0.275}_{\textit{2-bit}},$$
$$r_{\max} \approx \underbrace{0.007}_{\textit{8-bit}}, \underbrace{0.014}_{\textit{7-bit}}, \underbrace{0.028}_{\textit{6-bit}}, \underbrace{0.056}_{\textit{5-bit}}, \underbrace{0.113}_{\textit{4-bit}}, \underbrace{0.225}_{\textit{3-bit}}, \underbrace{0.275}_{\textit{2-bit}}.$$

B. Proofs

B.1. Proofs of Signal Swamping

Proof of Theorem 3.1. Notice that the quantization at $t+1$ update can be formulated as follows

$$\begin{aligned} q_{t+1} &= Q(\hat{x}_{t+1}) \\ &= Q(\beta \cdot \tilde{x}_t + (1-\beta) \cdot z_{t+1}) \\ &= Q(\beta \cdot y_{q_t} \cdot \Delta_t + (1-\beta) \cdot z_{t+1}) \\ &= \operatorname*{argmin}_{k=0}^{2^b-1} \big|\beta \cdot y_{q_t} \cdot \frac{\Delta_t}{\Delta_{t+1}} + (1-\beta) \cdot \frac{z_{t+1}}{\Delta_{t+1}} - y_k\big|. \end{aligned}$$

It can be easily derived that $q_{t+1} = q_t$ if

$$\big|\beta \cdot y_{q_t} \cdot \frac{\Delta_t}{\Delta_{t+1}} + (1-\beta) \cdot \frac{z_{t+1}}{\Delta_{t+1}} - y_{q_t}\big| \le r. \tag{19}$$

Remark that this condition is also necessary when $|y_{q_t} - y_{q_t-1}| = |y_{q_t+1} - y_{q_t}|$, *e.g.*, in the case of linear quantization.

Reranging the left hand side gives

$$\begin{aligned} &\big|\beta \cdot y_{q_t} \cdot \frac{\Delta_t}{\Delta_{t+1}} + (1-\beta) \cdot \frac{z_{t+1}}{\Delta_{t+1}} - y_{q_t}\big| \\ =&\big|\beta(\frac{\Delta_t}{\Delta_{t+1}} - 1)y_{q_t} + (1-\beta)(\frac{z_{t+1}}{\Delta_{t+1}} - y_{q_t})\big| \\ \le&\Big|\frac{\Delta_t}{\Delta_{t+1}} - 1\Big| + (1-\beta) \cdot \Big|\frac{z_{t+1}}{\Delta_{t+1}} - y_{q_t}\Big|. \end{aligned}$$

Therefore, the inequality (19) holds true as long as

$$\Big|\frac{\Delta_t}{\Delta_{t+1}} - 1\Big| + (1-\beta) \cdot \Big|\frac{z_{t+1}}{\Delta_{t+1}} - y_{q_t}\Big| \le r.$$

□

Corollary B.1 (A generalized version of Corollary 3.2)**.** *If $\Delta_{t+1} = \Delta_t$ and $r_t \ge 2(1-\beta)$, the unsigned quantized state q_t remains unchanged for any $z_{t+1} \le \Delta_t$. To be specific,*

- *For linear quantization, the received signals are swamped by states corresponding to any level when*

$$\textit{Unsigned: } \beta \gtrapprox \underbrace{0.999}_{\textit{8-bit}}, \underbrace{0.967}_{\textit{4-bit}}, \underbrace{0.929}_{\textit{3-bit}}, \underbrace{0.833}_{\textit{2-bit}}; \quad \textit{Signed: } \beta \gtrapprox \underbrace{0.998}_{\textit{8-bit}}, \underbrace{0.965}_{\textit{4-bit}}, \underbrace{0.917}_{\textit{3-bit}}, \underbrace{0.750}_{\textit{2-bit}}. \tag{20}$$

- *For dynamic exponent quantization, the received signals are swamped by states corresponding to half of the levels when*

$$\textit{Unsigned: } \beta \gtrapprox \underbrace{0.998}_{\textit{8-bit}}, \underbrace{0.966}_{\textit{4-bit}}, \underbrace{0.933}_{\textit{3-bit}}, \underbrace{0.837}_{\textit{2-bit}}; \quad \textit{Signed: } \beta \gtrapprox \underbrace{0.998}_{\textit{8-bit}}, \underbrace{0.967}_{\textit{4-bit}}, \underbrace{0.933}_{\textit{3-bit}}, \underbrace{0.863}_{\textit{2-bit}}. \tag{21}$$

Proof. According to the proof of Theorem 3.1, we know the quantized state becomes swamped if

$$(1-\beta)\cdot\left|\frac{z_{t+1}}{\Delta_{t+1}}-y_{q_t}\right|\leq r. \tag{22}$$

It provides two sufficient conditions for the unsigned and signed cases, respectively; that is,

$$\beta\geq\begin{cases}1-r_{\min} & \text{if } unsigned,\\ 1-r_{\min}/2 & \text{if } signed.\end{cases} \tag{23}$$

The results then follow from the Fact A.1. □

B.2. Proof of Proposition 3.4

We first present a trivial lemma regarding a two-point distribution.

Lemma B.2. *Let X be a random variable with*

$$\mathbb{P}[X=a]=p,\quad \mathbb{P}[X=b]=q=1-p. \tag{24}$$

Then, we have

$$\mathbb{E}[X]=pa+qb,\quad \mathbf{Var}[X]=pq(a-b)^2. \tag{25}$$

Proof. The proof is obvious. □

Proof of Proposition 3.4. For a $y_{k-1}\leq x/\Delta\leq y_k$, we have

$$\frac{1}{\sqrt{\hat{x}}}=\begin{cases}\frac{\Delta}{\sqrt{y_{k-1}}}, & w.p.\ \ \frac{y_k-x/\Delta}{y_k-y_{k-1}},\\ \frac{\Delta}{\sqrt{y_k}}, & w.p.\ \ \frac{x/\Delta-y_{k-1}}{y_k-y_{k-1}}.\end{cases}$$

Applying Lemma B.2 with $p=\frac{y_k-x/\Delta}{y_k-y_{k-1}}, a=\frac{\Delta}{\sqrt{y_{k-1}}}, b=\frac{\Delta}{\sqrt{y_k}}$, we have

$$\mathbf{Var}(\frac{1}{\sqrt{\hat{x}}})=\frac{(y_k-x/\Delta)(x/\Delta-y_{k-1})}{(y_k-y_{k-1})^2}\cdot\Big(\frac{\Delta}{\sqrt{y_{k-1}}}-\frac{\Delta}{\sqrt{y_k}}\Big)^2.$$

The proof is finished by noting the fact that the magnitude of the first term is determined by the relative distance x/Δ within the interval $[y_{k-1},y_k]$. □

B.3. Proof of Proposition 3.5

For an intermediate state value of $q_t=(\beta^c)^{k+k'}$, the state transition probability after receiving a zero-value signal ($z_{t+1}=0$) can be represented as follows:

$$q_{t+1}=\begin{cases}(\beta^c)^{k+k'}, & w.p.\ \ \frac{c-1}{c},\\ (\beta^c)^{k+k'+1}, & w.p.\ \ \frac{1}{c}.\end{cases} \tag{26}$$

Thus, transitioning from the state value of $(\beta^c)^k$ to $(\beta^c)^{k+s}$ needs exact s independent successes. Denoted by N the counting of updates required to achieve exact s successes, this random variable N adheres to a negative binomial distribution with a success probability of $1/c$. It has been proved in the majority of standard statistical textbooks that

$$\mathbb{E}\big[(\beta^c)^k\xrightarrow{\text{Ours}}(\beta^c)^{k+s}\big|z\equiv 0\big]=\mathbb{E}[N]=\frac{s}{1/c}=c\cdot s. \tag{27}$$

B.4. Proof of Theorem 3.6

Revisting the quantized EMA update, we have

$$\begin{aligned}\hat{x}_{t+1}&=\beta\cdot\tilde{x}_t+(1-\beta)\cdot g_{t+1}\\ &=\beta\cdot(\hat{x}_t+\tilde{x}_t-\hat{x}_t)+(1-\beta)\cdot g_{t+1}\\ &=\beta\cdot\hat{x}_t+(1-\beta)\cdot\Big(\underbrace{g_{t+1}+\frac{\beta}{1-\beta}(\tilde{x}_t-\hat{x}_t)}_{=:\tilde{g}_{t+1}}\Big).\end{aligned}$$

Since standard stochastic rounding is applied independently in each update, the quantization error can be treated as noise within the gradient. Denote $x_t := \hat{x}_t$, yielding a standard EMA update:

$$x_{t+1} \leftarrow \beta \cdot x_t + (1-\beta) \cdot \tilde{g}_{t+1}.$$

$\mathbb{E}[\tilde{g}_{t+1}] = \mathbb{E}[g_{t+1}]$ is obvious because of the zero expectation of quantization noise, and we are to establish its variance next, or equivalently

$$\mathbf{Var}\Big[\frac{\beta}{1-\beta}(\tilde{x}_t - \hat{x}_t)\Big] = \Big(\frac{\beta}{1-\beta}\Delta_t\Big)^2 \mathbf{Var}[y_{q_t} - \frac{\hat{x}_t}{\Delta_t}] = \Big(\frac{\beta}{1-\beta}\Delta_t\Big)^2 \mathbf{Var}[y_{q_t}]. \tag{28}$$

Without loss of generality, suppose $y_{k-1} \leq \hat{x}_t/\Delta_t \leq y_k$. It is easy to show that

$$\mathbf{Var}[y_{q_t}] = \frac{(y_k - x/\Delta)(x/\Delta - y_{k-1})}{(y_k - y_{k-1})^2} \cdot (y_{k-1} - y_k)^2 \tag{29}$$

by applying Lemma B.2 and noticing the fact that

$$y_{q_t} = \begin{cases} y_{k-1}, & w.p. \quad \frac{y_k - \hat{x}_t/\Delta_t}{y_k - y_{k-1}}, \\ y_k, & w.p. \quad \frac{\hat{x}_t/\Delta_t - y_{k-1}}{y_k - y_{k-1}}. \end{cases}$$

Then, we have

$$\mathbf{Var}\Big[\frac{\beta}{1-\beta}(\tilde{x}_t - \hat{x}_t)\Big] = \Big(\frac{\beta}{1-\beta}\Delta_t\Big)^2 \cdot \frac{(y_k - x/\Delta)(x/\Delta - y_{k-1})}{(y_k - y_{k-1})^2} \cdot (y_{k-1} - y_k)^2 \tag{30}$$

$$\leq \Big(\frac{\beta}{1-\beta}\Delta_t\Big)^2 \cdot \frac{1}{4} \cdot (y_{k-1} - y_k)^2 \tag{31}$$

$$\lessapprox \Big(\frac{\beta}{1-\beta}\Delta_t\Big)^2 \cdot \frac{1}{4} \cdot (2r_{\max})^2 = \Big(\frac{\beta}{1-\beta} r_{\max}\Delta_t\Big)^2, \tag{32}$$

where the first inequality is because

$$pq \leq \frac{1}{4} \quad \text{if } 0 \leq p, q \leq 1 \text{ and } p + q = 1,$$

and the second inequality holds true is due to the definition of $r_{\max}$.

C. Experimental Details

C.1. Settings and Hyperparameters

Hyperparameter	Value
LR	5e-4
Warmup LR	1.e-7
LR Scheduler	Inverse sqrt
Weight Decay	0
β_2	0.98
Max Steps	200,000
Warmup Steps	4,000
Label Smoothing	0.1
Dropout	0.3

Table 4. The hyperparameters of Transformer-base training on WMT'14 English-German translation.

Transformer-Base (♠) on WMT'14. We consider the Neural Machine Translation (NMT) task follow the paper (Ott et al., 2018) and the codebase[3]. We train a Transformer-Base model on the WMT'14 English-German translation task from

[3] https://github.com/NVIDIA/DeepLearningExamples/blob/master/PyTorch/Translation/Transformer

	MNLI	QNLI	QQP	RTE	MRPC	SST-2	COLA	STS-B
Batch Size	32	32	32	16	16	32	16	16
LR	1e-5	1e-5	1e-5	2e-5	1e-5	1e-5	1e-5	2e-5
Weight Decay	0.1	0.1	0.1	0.1	0.1	0.1	0.1	0.1
β_2	0.98	0.98	0.98	0.98	0.98	0.98	0.98	0.98
Warmup Steps	7,432	1,986	28,318	122	137	1,256	320	214
Max Steps	123,873	33,112	113,272	2,036	2,296	20,935	5,336	3,598
Max Seq. Len.	128	128	128	512	512	512	512	512

Table 5. The hyperparameters of RoBERTa-L fine-tuning on GLUE.

scratch. The specific setting can be found in Table 4. Four A800 GPUs have been used for the runs of tasks. We report the BLEU (Papineni et al., 2002) results (averaged over 3 independent runs) from the best checkpoint.

RoBERTa-Large (🔥) on GLUE. NLP fine-tuning plays a critical role in achieving satisfactory performance across specific scenarios. During the early stages of NLP development, downstream tasks could not be effectively addressed using a single model, thus giving rise to various specialized domains, including Natural Language Understanding (NLU), Question Answering (QA), and Natural Language Generation (NLG). This study evaluates the performance of a low-bit optimizer in NLU[4] by fine-tuning the RoBERTa-L model (Liu, 2019) on the widely utilized GLUE benchmark (Wang et al., 2018a), which supports 8 different tasks. Their respective experimental settings are listed in Table 5. Besides, a linear schedule is employed for learning rate decay. With the exception of SST-2, which necessitates two GPUs for execution, the results on the remaining datasets are obtained using a single RTX 3090 GPU.

Hyperparameter	Value
Batch Size	512
LR	5e-4
Weight Decay	0.05
Emb. Decay	0
β_2	0.999
Epochs	300

Table 6. The hyperparameters of Swin-T pretraining on ImageNet-1K.

Swin-T (💧) on ImageNet-1K. CV pretraining can provide a robust foundational model for a wide range of downstream tasks, among which image classification remains the most prevalent task for universal representation learning. To demonstrate the effectiveness of our approach in computer vision applications, we train the tiny variant of the Swin Transformer (Liu et al., 2021) from scratch on the ImageNet-1K dataset (Deng et al., 2009) for the image classification task[5]. Detailed experimental configurations are provided in Table 6. The training is conducted using four NVIDIA V100 GPUs. For evaluation, we report both top-1 and top-5 accuracy.

DCN (💧) on Criteo and HSTU-Large (💧) on MovieLens. RS training has garnered greater interest from the industrial community compared to NLP and CV scenarios. Moreover, recommender systems are well-known for their large-scale user and item entities, resulting in massive embedding tables. This makes them particularly valuable for study in this context, as their 'gigantic' nature arises not merely from deeper or wider model architectures, but from the scale of the entities themselves. We consider two primary tasks across the recommendation pipeline. Sequential recommendation focuses on retrieving a list of candidate items to be passed to the subsequent ranking stage. Click-Through Rate (CTR) prediction is a classical industrial application that estimates the probability of a candidate item being clicked. For the former, we adopt the recently proposed HSTU[6] model (Zhai et al., 2024) on the widely used MovieLens-1M dataset, while for the latter, we

[4] https://github.com/huggingface/transformers/tree/main/examples/pytorch/text-classification

[5] https://github.com/microsoft/Swin-Transformer

[6] https://github.com/facebookresearch/generative-recommenders

Hyperparameter	Value
Batch Size	4,096
LR	1e-3
Weight Decay	0
Emb. Decay	1e-5
β_2	0.999
Epochs	100

(a) DCN training on Criteo

Hyperparameter	Value
Batch Size	128
Num Negatives	128
LR	1e-3
Weight Decay	0
β_2	0.999
Epochs	100

(b) HSTU training on MovieLens

Table 7. The hyperparameters of RS training.

consider the classic DCN[7] model (Wang et al., 2017) on the Criteo dataset. The hyperparameters can be found in Table 7.

Hyperparameter	Value
Batch Size	120
LR	2e-5
Weight Decay	0
β_2	0.999
Warmup Ratio	0.03
Epochs	3

Table 8. The hyperparameters of LLaMA fine-tuning on Alpaca.

LLaMA-7B (🔥) on Alpaca. LLM fine-tuning is one of the most compelling applications, but still faces challenges due to its high memory demands. Since ChatGPT's pioneering days, a number of open source LLMs (Touvron et al., 2023; GenAI, 2023; Bai et al., 2023; Yang et al., 2024; Liu et al., 2024a;b) have been released, with the LLaMA series receiving the most attention. Hence, we fine-tune LLaMA-7B (Touvron et al., 2023) based on Alpaca (Taori et al., 2023) codebase[8] with the hyperparameters given in Table 8. Due to the utilization of three H800 GPUs for training, we adopt a total batch size of 120 instead of the standard 128, with 40 assigned to each GPU. For evaluation on the MMLU (Hendrycks et al., 2020) and standard common sense reasoning benchmarks: ARC easy and challenge (Clark et al., 2018), OpenBookQA (Mihaylov et al., 2018), and Social Interaction QA (Sap et al., 2019), we utlize OpenCompass (Contributors, 2023).

Hyperparameter	Value
Batch Size	120
LR	2e-5
Weight Decay	0
β_2	0.999
Warmup Ratio	0.03
Epochs	1
Visual Tower	clip-vit-large-patch14-336
Projector Type	mlp2x_gelu

Table 9. The hyperparameters of LLaVA-1.5 fine-tuning on a mixture instruction tuning data.

LLaVA-1.5 (🔥) visual instruction tuning. We follow the LLaVA-1.5 codebase[9] to fine-tune the Vicuna-7B-v1.5 model (Chiang et al., 2023) on a mixed instruction tuning dataset comprising COCO (Caesar et al., 2018), GQA (Hudson & Manning, 2019), OCR-VQA (Mishra et al., 2019), TextVQA (Singh et al., 2019), and VisualGenome (Krishna et al., 2017). Due to the use of three H800 GPUs for training, we employ a total batch size of 120 instead of the standard 128 by assigning a

[7] https://github.com/MTandHJ/RecBoard/tree/master/DCN
[8] https://github.com/tatsu-lab/stanford_alpaca
[9] https://github.com/haotian-liu/LLaVA

batch size of 40 to each GPU. All other hyperparameters adhere to the recommended configurations and have been detailed in Table 9. In accordance with the official evaluation protocols, we assess the fine-tuned models on several benchmarks, including ScienceQA (Lu et al., 2022), TextVQA (Singh et al., 2019), POPE (Li et al., 2023c), and MME (Fu et al., 2023). Specifically, we report accuracy for ScienceQA and TextVQA; the F1-score averaged across the 'Random', 'Adversarial', and 'Popular' subtasks for POPE; the 'Perception' score for MME.

D. 2nd State Distribution Visualization

Below, we illustrate the 2nd state distribution (over 8,192 entries of a linear layer) visualization on other models and tasks. This empirically corroborates the superiority of SOLO in approximating the dynamics of full-precision optimization.

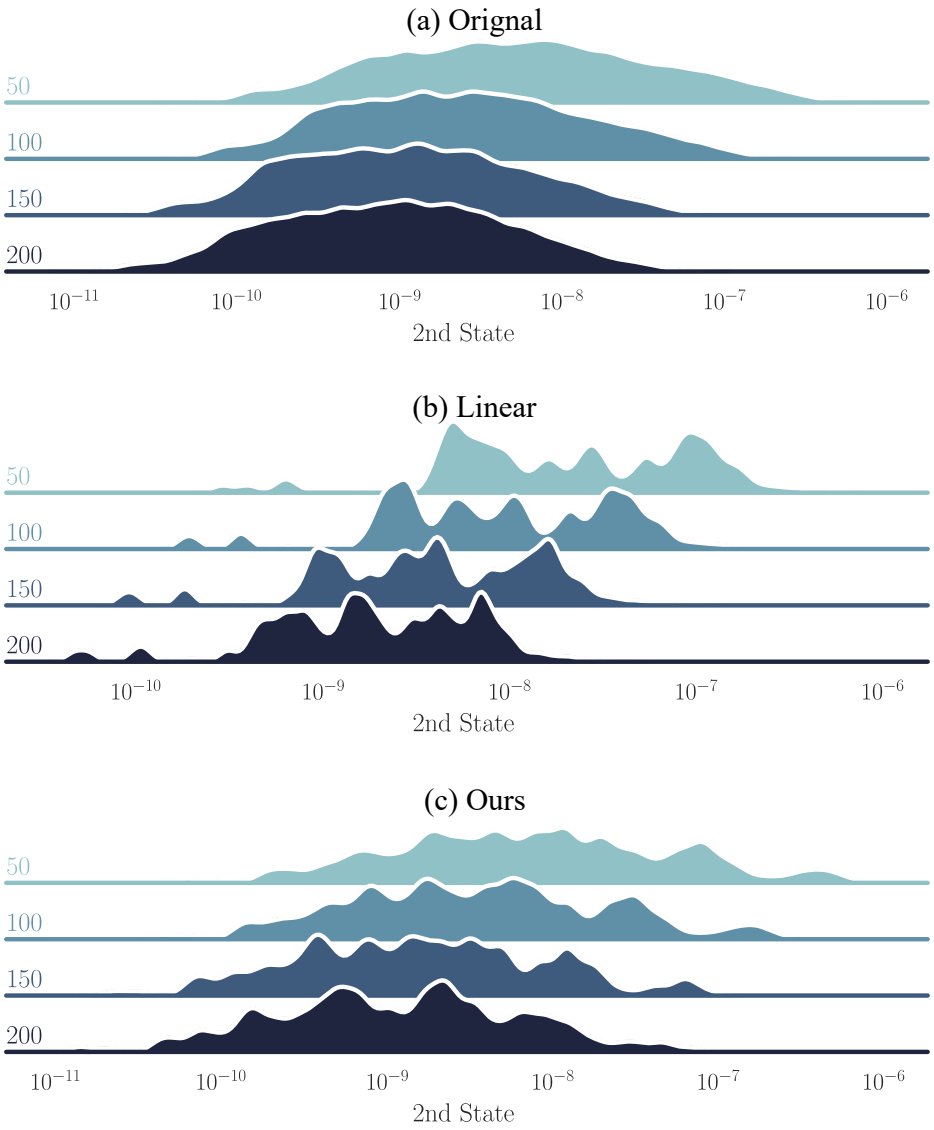

Figure 10. How the 2nd state distribution of Transformer-Base (🔥) changes at steps 50, 100, 150, and 200. DE quantization is omitted, as it leads to an immediate training collapse.

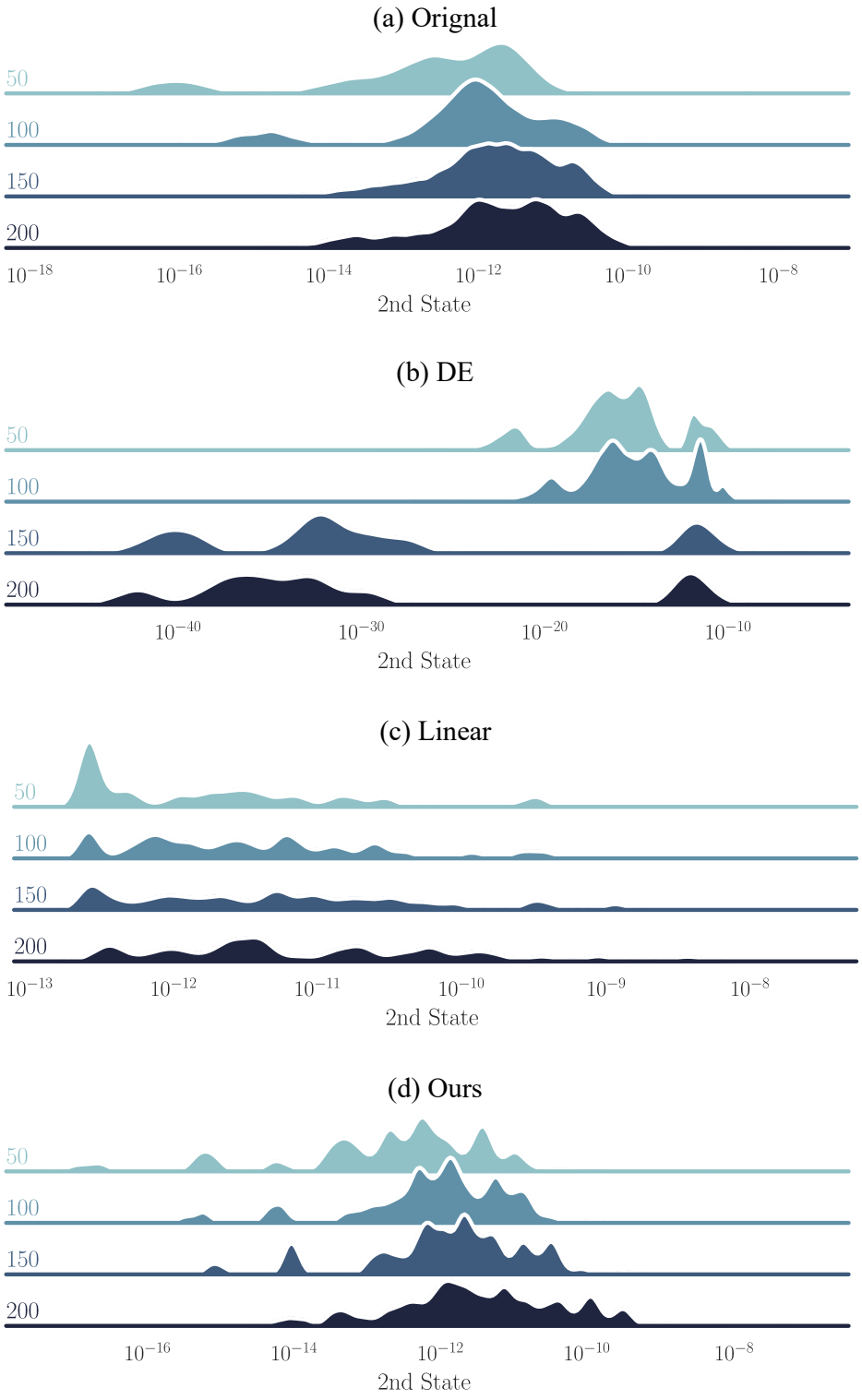

Figure 11. How the 2nd state distribution of RoBERTa-Large (🔥 on COLA) changes at steps 50, 100, 150, and 200.

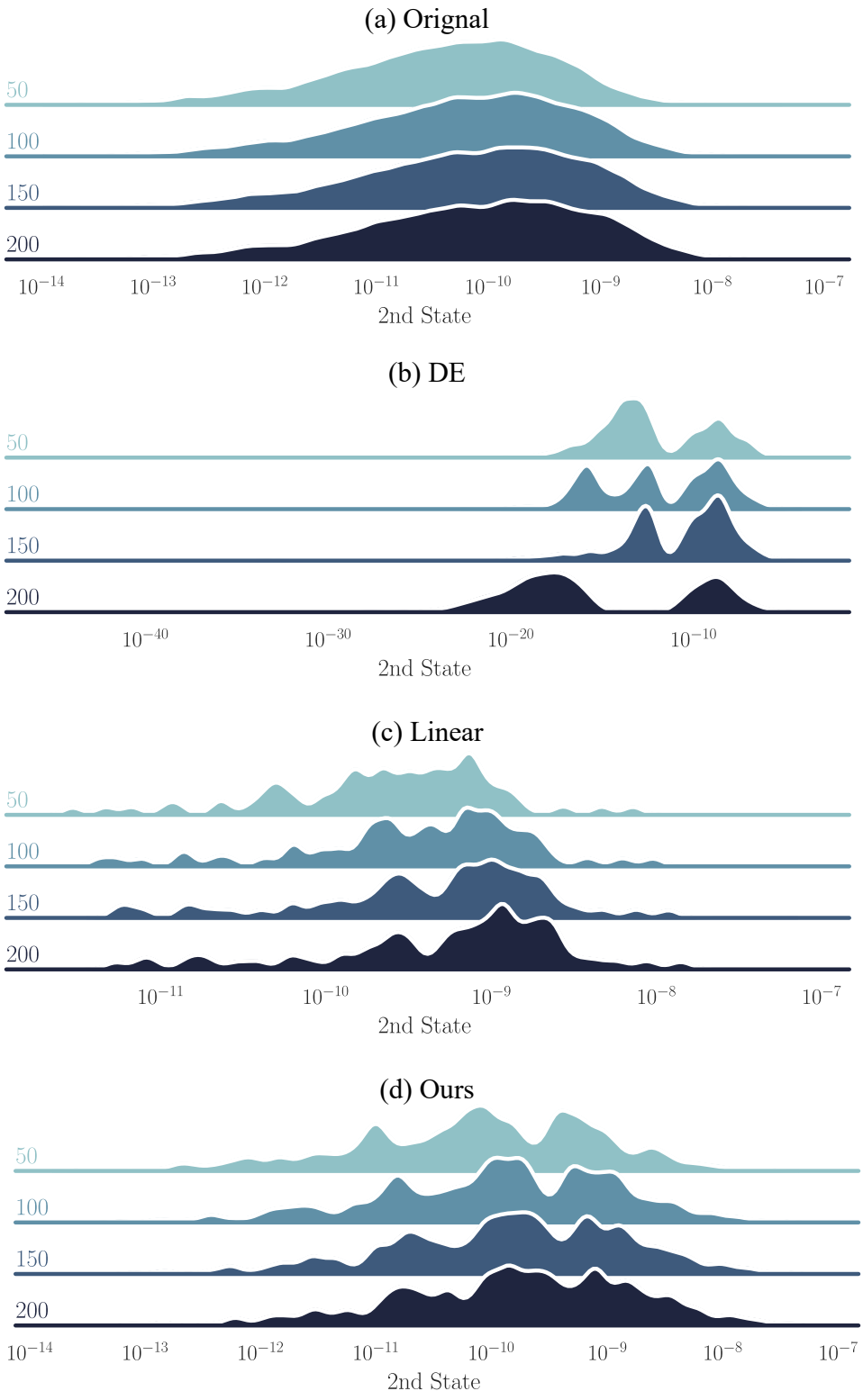

Figure 12. How the 2nd state distribution of DCN (🔥) changes at steps 50, 100, 150, and 200.

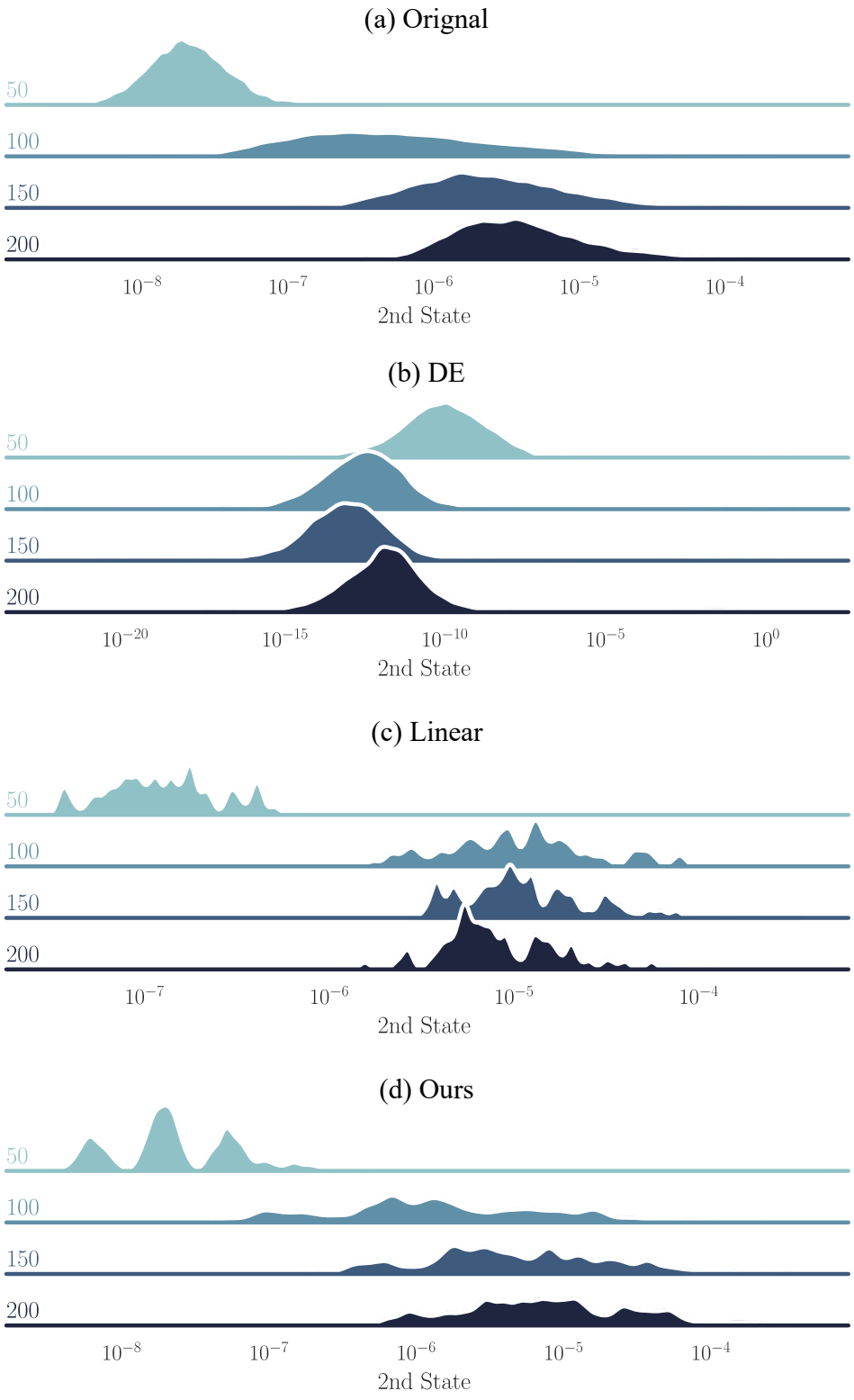

Figure 13. How the 2nd state distribution of HSTU (🔥) changes at steps 50, 100, 150, and 200.